Toward an understanding of disequilibrium dihedral angles in mafic rocks

Marian B. Holness,[1] Madeleine C. S. Humphreys,[2] Rachel Sides,[1] Rosalind T. Helz,[3] and Christian Tegner[4]

[1]   The median dihedral angle at clinopyroxene-plagioclase-plagioclase junctions in mafic rocks, Θ_{cpp}, is generally lower than equilibrium ($109° \pm 2°$). Observation of a wide range of mafic bodies demonstrates that previous work on systematic variations of Θ_{cpp} is incorrect in several important respects. First, the spatial distribution of plagioclase compositional zoning demonstrates that the final geometry of three-grain junctions, and hence Θ_{cpp}, is formed during solidification (the igneous process): sub-solidus textural modification in most dolerites and gabbros, previously thought to be the dominant control on Θ_{cpp}, is insignificant. Θ_{cpp} is governed by mass transport constraints, the inhibiting effects of small pore size on crystallization, and variation in relative growth rates of pyroxene and plagioclase. During rapid cooling, pyroxene preferentially fills wider pores while the narrower pores remain melt-filled, resulting in an initial value of Θ_{cpp} of $78°$, rather than $60°$ which would be expected if all melt-filled pores were filled with pyroxene. Lower cooling rates create a higher initial Θ_{cpp} due to changes in relative growth rates of the two minerals at the nascent three-grain junction. Low Θ_{cpp} (associated with cuspate clinopyroxene grains at triple junctions) can also be diagnostic of infiltration of previously melt-free rocks by late-stage evolved liquids (the metasomatic process). Modification of Θ_{cpp} by sub-solidus textural equilibration (the metamorphic process) is only important for fine-grained mafic rocks such as chilled margins and intraplutonic chill zones. In coarse-grained gabbros from shallow crustal intrusions the metamorphic process occurs only in the centers of oikocrysts, associated with rounding of chadacrysts.

Citation: Holness, M. B., M. C. S. Humphreys, R. Sides, R. T. Helz, and C. Tegner (2012), Toward an understanding of disequilibrium dihedral angles in mafic rocks, *J. Geophys. Res.*, *117*, B06207, doi:10.1029/2011JB008902.

1.   Introduction

[2]   The relative orientations of grain boundaries at three-grain junctions in many rocks bear little relationship to those expected for textural equilibrium [e.g., *Sawyer*, 1999; *Kruhl and Peternell*, 2002; *Holness et al.*, 2005a]. Disequilibrium is even common at three-grain junctions between grains of the same phase, despite this type of junction being sensitive to recrystallization [*Voll*, 1960]: while geometry dictates that the population of such angles must have a median of 120° (consistent with equilibrium), the spread of angles around this median value is generally too great [e.g., *Liebl et al.*, 2007] and true equilibrium is only attained at high metamorphic grades. Recent work has shown that disequilibrium angle populations, particularly those formed at clinopyroxene-plagioclase-plagioclase junctions (abbreviated to cpx-plag-plag) are ubiquitous in mafic layered intrusions [*Holness*, 2005, 2007; *Holness et al.*, 2007a]. Systematic spatial variation of cpx-plag-plag disequilibrium angles has been used qualitatively to identify recharge in magma chambers [*Holness*, 2005, 2007; *Holness et al.*, 2007a; *Holness and Winpenny*, 2009], place constraints on the thickness of the crystal mushy layer on magma chamber floors [*Holness et al.*, 2007a], and as a diagnostic of infiltration [*Holness*, 2007]. Here we offer a new description of the creation and subsequent evolution of disequilibrium dihedral angles that is essential if we are to use this new petrographic parameter to place quantitative constraints on the time-scales of igneous and metamorphic processes.

[3]   The starting point for the present contribution is recent work that highlighted the extent and significance of primary chemical zoning in the outermost margins of plagioclase grains in the Skaergaard Layered Series [*Toplis et al.*, 2008; *Humphreys*, 2009, 2011]. Detailed examination of three-grain junctions shows that these compositional differences

[1]Department of Earth Sciences, University of Cambridge, Downing Street, Cambridge, UK.

[2]Department of Earth Sciences, University of Oxford, South Parks Road, Oxford, UK.

[3]U.S. Geological Survey National Center, Reston, Virginia, USA.

[4]Department of Earth Sciences, University of Aarhus, Aarhus, Denmark.

Corresponding author: M. Holness, Department of Earth Sciences, University of Cambridge, Downing Street, Cambridge CB2 3EQ, UK. (marian@esc.cam.ac.uk)
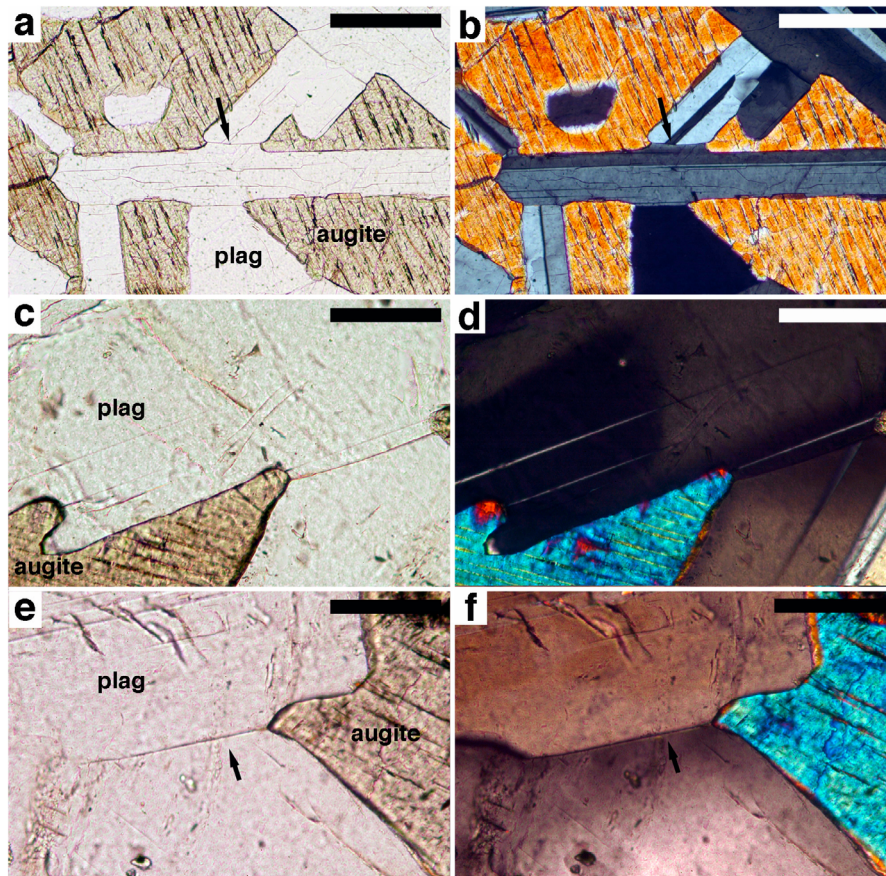
Figure 1. Photomicrographs of gabbros from the Lower Zone of the Skaergaard intrusion, East Greenland showing details of junctions between augite (pale brown in plane polarized light) and plagioclase (clear in plane polarized light). (a and b) Sample labeled 1009′11″ from 307.8 m depth in the Cambridge 1966 drill core, collared near the coast at Uttental Plateau, showing the common asymmetry of augite-plagioclase-plagioclase junctions. One grain boundary is marked by a zone of compositionally distinct plagioclase (arrowed). Scale bars are 200 μm long. The rest of the images are pairs of photomicrographs (taken in plane polarized light and with crossed polars) that show the geometry of the cpx-plag-plag junctions and the zone of anorthitic plagioclase formed in the immediate vicinity of the junction. All samples are from Uttental Plateau and have been previously described by *Tegner et al.* [2009] and *Holness et al.* [2007b]. (c and d) Sample 458219. Note the marked asymmetry of the junction, formed by the meeting of a curved augite-plagioclase boundary with a planar augite-plagioclase boundary. Note the distinct compositional zoning of the plagioclase at the plagioclase-plagioclase grain boundary. Scale bars in each are 100 μm long. (e and f) Sample 458242. Only one plagioclase grain has clearly visible zoning (arrowed). Scale bars in each are 100 μm long.

occur in the immediate vicinity of augite-plagioclase-plagioclase junctions in the Skaergaard cumulates (Figure 1). In LZa, the outermost parts of plagioclase grains can be more anorthitic than the cores, but commonly only one of the two plagioclase grains meeting at any augite-plagioclase-plagioclase junction will exhibit reverse zoning (Figures 1b and 1f). Diffusive re-distribution of Na and Ca in chemically zoned plagioclase is very sluggish [*Grove et al.*, 1984], so it is unlikely that this zonation could be a metamorphic overprint. In addition, one of the plagioclase-augite grain boundaries may show marked curvature while the other is planar – the plagioclase grain forming the curved boundary is commonly that with the anorthitic rim. While curved grain boundaries at three-grain junctions in (texturally equilibrated) quartzites may be a consequence of anisotropy of interfacial energies [*Kruhl*, 2001], we doubt that anisotropy

is playing a systematic role in the Skaergaard gabbros both because there is no apparent relationship with augite orientation, and because the observed geometries are far from those expected for textural equilibrium. The preserved geometry of three-grain junctions in the Skaergaard gabbros is essentially unmodified from that formed *during* solidification, and must therefore be controlled by the kinetics of mass transport and crystal growth in the progressively occluded pore spaces within the crystal mush.

[4] This conclusion necessitates a re-interpretation of cpx-plag-plag disequilibrium populations in layered intrusions and a revision of explanations of their observed systematic variation. Previous work was based on the assumption that, immediately post-solidification, all mafic rocks contain essentially the same initial cpx-plag-plag dihedral angle population, created during solidification and characterized by a

median of ~60° and a high standard deviation. This initial dihedral angle population was then thought to be variably modified in the sub-solidus, with a greater approach to sub-solidus textural equilibrium (and higher dihedral angles) in rocks that stayed hot for a long time [*Holness et al.*, 2005a, 2007a, 2007b]. Our new observations demonstrate that, at least in the Skaergaard, the observed variations in angle through the Layered Series were formed *during* the actual process of creating the three-grain melt-free junction between the plagioclase and augite, and do not reflect differences in the sub-solidus cooling history. This new interpretation has major implications for the development of dihedral angles as a quantitative tool for decoding igneous and metamorphic processes, creating a clear division between processes operating within the crystal mush (liquid-present) and those operating in the sub-solidus.

[5] Quantifying exactly how solidification results in any given value of dihedral angle necessitates understanding how three-grain junctions are formed in a solidifying system. This problem can be broken down into a series of related questions: what happens when three grains meet during solidification?; how do extrinsic (temperature, time) and intrinsic (compositional) factors affect the replacement of liquid as three grains meet to form a mutual junction?; how much does sub-solidus modification affect triple junction geometries that formed during solidification, and what are the processes by which this occurs?

[6] There is an abundant literature on the subject of formation of grain boundaries and triple junctions, but much of this concerns numerical models of late-stage solidification [e.g., *Rappaz et al.*, 2003; *Echebarria et al.*, 2004; *Vernede and Rappaz*, 2007]. An alternative approach to understanding the solidification of mafic magmas is to undertake a detailed examination of partially solidified natural examples. In this contribution we describe a synthesis of new observations and data from a wide variety of mafic igneous rocks, discussing previously published work where necessary. We provide a new framework in which to understand the variation of disequilibrium dihedral angles in mafic rocks and the observational basis for a firm quantitative understanding of disequilibrium three-grain junctions. We concentrate on cpx-plag-plag junctions, although we anticipate that similar results would be found for any two-phase three-grain junction in solidifying systems. The answers we suggest to some of the questions posed above necessitate a re-evaluation of the current hypothesis for angle variations and lead us to postulate that much of the reported variation of dihedral angles in gabbros and dolerites is primary, resulting from processes acting during the initial formation of the three-grain junctions. Dihedral angle variation therefore encodes information about the later stages of solidification (when only a few vol.% liquid remains). Our new conceptual framework distinguishes between three-grain junctions created during solidification, those formed consequent to the introduction of late-stage liquids into solidified rock, and junctions modified in the absence of melt/liquid in response to sub-solidus textural equilibration.

[7] The distinctions between three-grain junction geometries created in these different environments were created *ab initio* from direct observation. It would be easy for the reader to lose their way through the large number of different geological case studies we must describe in order to reach

our conclusions. To prevent this, and to provide a guide through the mass of new observations and data, we have given the paper an unusual structure. Instead of describing all the geological examples at the start of the paper, we introduce each set of examples, or each individual case study, at the point in the narrative where it becomes relevant. The overall structure of the paper is fourfold: after a summary of previous work it is divided into sections on equilibrium, on the primary formation of dihedral angles (the *igneous process*), on the formation of low dihedral angles as a consequence of melt infiltration (the *metasomatic process*), with a final section on the modification of dihedral angles in the sub-solidus (the *metamorphic process*).

2. Previous Work on Disequilibrium Dihedral Angles

[8] A theoretical study by *Elliott et al.* [1997] involved the creation of artificial microstructures by increasing the size of cubic and lath-shaped crystals until impingement. Because the median of the resultant population cannot be anything other than 120°, it is the standard deviation that provides the useful information: this is 20°. The similarity of this value to that of a specimen of brass annealed for 1 h at 500°C [*Harker and Parker*, 1945] led Elliott et al. to conclude that their models are a good approximation to (disequilibrium) microstructures in monomineralic systems controlled entirely by euhedral crystal growth from a liquid. This result might also be applicable to metamorphic rocks. During reaction, dihedral angles between grains of the product phases are most likely to be controlled by the expediencies of crystal growth and replacement: angles will be determined more by the growth of kinetically favored crystal faces, rather than by interfacial energies.

[9] *Liebl et al.* [2007] pointed out that microstructural evolution during metamorphism can result in a change in the standard deviation of dihedral angle populations. *Voll* [1969] found that the angles between grain boundaries at quartz-quartz-quartz junctions in sedimentary rocks range from <60° to 180° around the median of 120°. The spread of angles decreases during metamorphism - deformed quartz aggregates that have undergone dynamic recrystallization and annealing have a narrower spread of 65–178° [*Liebl et al.*, 2007]. This is reduced even further (to 97–144°) in texturally equilibrated granulites [*Vernon*, 1968]. A similar result was observed in annealed sulphides [*Stanton and Gorman*, 1968]. The reduction in the spread of angles is therefore a measure of textural equilibration and has potential for quantification of thermal histories. A change in the spread of angles occurs at constant grain size in sulphides [*Stanton and Gorman*, 1968] suggesting, together with the observation that normal grain growth occurs in materials with equilibrium (or close to equilibrium) angle populations, that the grain junctions sort themselves out very early in the evolution of the microstructure [*Kruhl*, 2001; *Higgins*, 2011].

[10] An example in which post-reaction grain growth was likely to have had minimal effect on grain morphology, therefore permitting observation of dihedral angle change, is provided by forsterite marbles in the aureole of the Beinn an Dubhaich granite. Forsterite shape changes with distance from the forsterite-in isograd [*Holness et al.*, 1989]. At the isograd many grains are cuspate and irregular, while those

closer to the granite are rounded. This morphological change is accompanied by an increase in the median forsterite-calcite-calcite dihedral angle from 105° to 165°. The low median values near the isograd have been interpreted as a consequence of the olivine pseudomorphing an original fluid-filled porosity [*Holness et al.*, 1989, 1991] but they may preserve an early disequilibrium population formed during rapid reaction. The variation of angles toward the contact is interpreted as progressive textural equilibration via a diffusive process [*Holness et al.*, 1991], although there may also have been some control on the original shape formed during reaction by kinetic roughening caused by large overstep in the inner aureole [*Roselle et al.*, 1997].

[11] Work on dihedral angles in igneous rocks has primarily been focused on establishing the equilibrium value of melt-solid-solid angles (see the recent review in *Holness* [2010]), with little corresponding work on disequilibrium angles. Melt-solid-solid dihedral angles in a suite of glassy crystalline nodules form a continuous progression from that expected for purely growth-controlled microstructures toward textural equilibrium, suggestive of a continuous process of angle change during textural equilibration in melt-present systems [*Holness et al.*, 2005a]. A similar hypothesis has been put forward for fully solidified gabbros: *Holness et al.* [2005a] suggested that, immediately after solidification, the dihedral angle population of interstitial phases in gabbros is one of impingement (with a median of 60° and a high standard deviation). They reported a continuous array of angle populations between this impingement microstructure and complete solid-state textural equilibrium, and interpreted this as a consequence of progressive grain boundary migration at the fully formed (melt-free) three-grain junctions. According to this model, rocks with median dihedral angles of 60° and high standard deviation are those that cooled quickly once they had fully solidified, while those with angle populations approaching equilibrium are those which remained hot in the sub-solidus for a long time, permitting extensive diffusion-controlled equilibration in the sub-solidus.

[12] Pseudomorphing of an originally melt-filled porosity is also suggested as the process resulting in cuspate grains with low dihedral angles commonly observed in solidified melt pools in migmatites [e.g., *Platten*, 1982; *Harte et al.*, 1993; *Sawyer*, 1999; *Clemens and Holness*, 2000; *Holness and Sawyer*, 2008]. *Holness and Sawyer* [2008] suggested the cuspate shape is a consequence of the effect of pore size on crystal nucleation and growth. Delayed crystal growth in the smallest pores means the liquid tends to crystallize by initial overgrowth of the pore walls, followed by nucleation and growth of another phase in the remaining pore space [*Holness and Sawyer*, 2008]. If there is sufficient delay before the pore is pseudomorphed, textural equilibration may occur, leading to the pseudomorph inheriting a low dihedral angle and thus the cuspate grain shape typical of migmatites.

[13] Previously published work is insufficient to provide information on the processes underpinning the observed variations in dihedral angle. Without understanding the relevant processes we cannot construct theoretical models or provide robust quantitative relationships between dihedral angle variation and rock history. To create a more complete picture we need to look at a wider range of geological environments.

2.1. Measurement of Dihedral Angles

[14] Key to everything we describe is an accurate, robust and reproducible method of measuring and reporting dihedral angle data. Most published work reports the median of populations, primarily because the median can be determined to within a few degrees with a relatively small number of individual measurements [*Riegger and van Vlack*, 1960]. Much of the early work on dihedral angles in geological systems followed the lead of metallurgists and was based on populations of apparent angles measured on a flat rotating stage (although see *Voll* [1960] and *Vernon* [1968] for exceptions). However, there is much important information to be obtained from the population of true angles in a sample. Measurement therefore needs to be done on a universal stage.

[15] There are several possible sources of error in determining the dihedral angle population. The first is a simple measurement bias, with undue emphasis given to angles in a particular size range. The universal stage provides a useful check on this possibility, since the observer does not generally know what the angle looks like until some effort has been expended in orienting the junction correctly. Another source of error is that associated with an individual measurement, and this is typically of the order of a few degrees [e.g., *Gleason et al.*, 1999]. The final source of error is more complex. Because we don't know the distribution function of the underlying (parent) population that is being sampled, it is not straightforward to work out the error on the median or standard deviation of a population of measured angles. *Stickels and Hücke* [1964] developed a non-parametric method, based on the assumption that the population has a continuous distribution function of some unknown form, to establish a confidence interval for the median angle of a population independent of its actual distribution. *Holness* [2010] showed, by generating at random small populations from a much larger parent population, that for rocks in which the texture is at, or close to, textural equilibrium (for which the standard deviation is generally <15° [*Holness et al.*, 2005a]), the true value of the median is likely to be closely approached (i.e., a 95% confidence interval of ±2°) if 100 individual angles are measured. The median of 100 measurements of a sample far from equilibrium (with a standard deviation >20°, such as expected for melt-bearing systems undergoing rapid solidification [*Holness et al.*, 2005a]) is likely only to be correct within ±6°. In this study, we have obtained 100 individual measurements of dihedral angle from most samples, examining more than one thin-section if necessary. We use the method of *Stickels and Hücke* [1964] to constrain the 95% confidence interval on the median, and report both the standard deviation and the skew of our measured populations. The full data sets are available in the auxiliary material.[1]

3. Equilibrium Dihedral Angles

[16] Any discussion of disequilibrium microstructures must first begin with a description of equilibrium.

---

[1]Auxiliary materials are available at ftp://ftp.agu.org/apend/jb/2011jb008902.
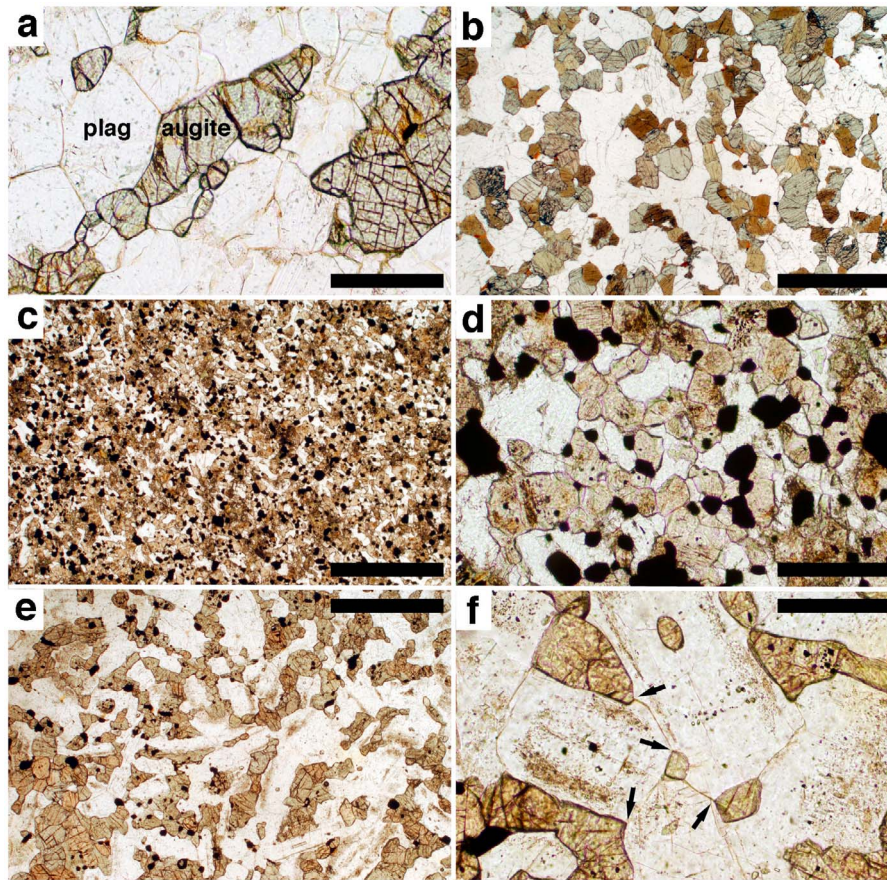
Figure 2. Photomicrographs of equilibrated microstructures in augite-plagioclase rocks. Augite is pale brown/green in all images, while plagioclase is colorless. All sample numbers (apart from V5) denote the Harker Collection number. (a) Sample 51465. A granulitic norite, with smoothly rounded plagioclase-augite grain boundaries denoting a close approach to textural equilibrium. Scale bar is 200 μm long. (b) Sample 94400. Recrystallized gabbro from Quebec. This sample contains appreciable amounts of hornblende, as well as two pyroxenes, but is characterized by an almost unimodal grain size, together with smooth grain boundaries. Scale bar is 1 mm long. (c and d) V5 – this two-pyroxene hornfels formed by recrystallization of the basaltic lava flow which forms part of the eastern wall of the Skaergaard intrusion. Note the randomly oriented elongate plagioclase grains in Figure 2c, presumably relict from the original basaltic microstructure. Scale bar is 1 mm long. In Figure 2d the microstructure is now mostly fine-grained and equigranular. Scale bar is 200 μm long. (e and f) Sample 114425 from the chilled margin of the Bushveld Complex. In Figure 2e the relict plagioclase shape is evident, with abundant randomly oriented laths. There are two pyroxenes in this rock, augite (pale green) and hypersthene (green-pink pleochroic). Scale bar is 1 mm long. In detail (Figure 2f) the augite grains are rounded with smooth grain boundaries. Note the high dihedral angles (arrowed). Scale bar is 200 μm long.

Equilibrium cpx-plag-plag dihedral angles are described by *Vernon* [1968, 1970] and *Holness et al.* [2005a]. The median values range from 108° to 122°, with standard deviations of 11–17°. The wide range of published values prompted a re-examination: we assembled a collection of rocks from the Harker Collection (University of Cambridge) that exhibit the expected microstructure of a fully texturally equilibrated rock (approximately unimodal grain size, smoothly curved or straight grain boundaries and an overall granular texture. Figure 2), and re-measured the single sample described by *Holness et al.* [2005a].

[17] The re-measured sample is 11787, a two-pyroxene granulite from Perugar, Madura district, South India. The new samples are: 51465 - a granulitic norite from Devabhumi Quarries, Ganjam district, Madras Presidency (modern state of Orissa), India (Figure 2a); 52047 – a pyroxene granulite from Chemnitzbach, near Mohsdorf, Saxony (modern Land Sachsen), Germany; 94399 and 94400 – recrystallized gabbro from the Morin Series, SE. Grenville township, Province Quebec, Canada [*Philpotts*, 1963] (Figure 2b); V5 – basaltic hornfels from the eastern contact aureole of the Skaergaard Intrusion, East Greenland (Figures 2c and 2d); and 114425 – fine-grained gabbro from the chilled margin of the Bushveld Complex, South Africa (Figures 2e and 2f). The Grenville Province material is a high-grade metamorphic rock with a complex and poly-phase metamorphic history, completely recrystallized from the original basalt, but the fine-grained gabbro from the Bushveld retains much of the original

Table 1. Cpx-Plag-Plag Dihedral Angle Populations in Equilibrated Plagioclase-Augite Rocks

Sample	n^a	Median[b] (Θ_{cpp})	Standard Deviation	Skew
11787	200	113 ± 2	11.0	−0.1
51465	100	109 ± 2.5	10.1	0.4
52047	100	110 ± 2	9.0	−0.3
94399	50	107.5 ± 4.5	12.0	0.2
94400	50	109.5 ± 4	9.7	0.9
94399 + 94400	100	108.5 ± 3	10.9	0.4
114425	100	107 ± 2.5	9.7	0.2
V5	100	109 ± 2	9.2	0.4

[a]The number of measurements per sample.
[b]The error on the median is the 95% confidence interval calculated using the method of *Stickels and Hücke* [1964].

igneous microstructure (notably the shape and orientation of the plagioclase grains). Details of the dihedral angle populations in each of these samples are given in Table 1.

[18] The two samples of recrystallized gabbro from the Morin Series of Quebec are rather altered and it was not possible to measure 100 angles in each of the two available thin-sections, making our values of standard deviation rather inaccurate [*Holness*, 2010]. We compared the two populations using the Kolmorogov-Smirnov test (a non-parametric test to determine the likelihood that two data sets come from the same underlying population) and obtained a D value of 0.1533 and a probability of 73.4% that the two measured populations come from the same underlying population. As a comparison, the data sets for 51465 and 52047 give a D value of 0.09 and a probability of 79.4% that the two sets were from the same underlying population (i.e., a fully texturally equilibrated population). We therefore amalgamated the two Quebec data sets to make a single set with 100 measurements (Table 1).

[19] The medians and standard deviations of dihedral angle in these rocks are very similar, despite their different settings. However, they differ from the values reported by *Vernon* [1968, 1970]. The standard deviation of sample 11787 is significantly lower than that reported by *Holness et al.* [2005a] although the median is similar. The new results suggest that texturally equilibrated populations of cpx-plag-plag dihedral angles from a variety of different geological settings have a median value of ∼109° and a standard deviation of ∼10°. The skew of the population is small and generally positive.

4. Dihedral Angles Formed During Solidification: The Igneous Process

[20] To understand the formation of cpx-plag-plag angles, we must constrain the detailed geometry of plagioclase-plagioclase junctions in melt-bearing systems because, despite the simultaneous crystallization of clinopyroxene (generally augite) and plagioclase on a cotectic, we need two touching plagioclase grains to form the cpx-plag-plag dihedral angle. We can observe the controls on the formation of this primary plagioclase framework by examining glass-bearing crystalline nodules entrained in lava flows [e.g., *Holness et al.*, 2007c; *Martin et al.*, 2006]. Once the

framework is in place, continued crystallization of both augite and plagioclase results in solidification of the pore. A window into this aspect of solidification is provided by glass-bearing samples retrieved by successive drilling of lava lakes, where both spatial and temporal information is available. The timescales for solidification of these bodies is 10–100 years, substantially less than for layered intrusions. In the following sections we outline the progressive evolution of microstructures during solidification, concentrating on the formation of cpx-plag-plag junctions, deduced from close observation of suites of samples from the Kilauea Iki lava lake [*Helz et al.*, 1984; *Helz*, 1987; *Barth et al.*, 1994], and supplemented by samples of glassy andesitic and andesitic basalt nodules entrained in the Kameni lava flows of Santorini (see *Martin et al.* [2006] and *Holness et al.* [2005a] for further details), and samples of crystal clots entrained in lavas [*Holness*, 2006].

4.1. The Initial Plagioclase Framework

[21] Observation of plagioclase-rich rocks containing a high volume fraction of melt (glass) demonstrates there are three possible end-member microstructures.

[22] The first case is when the under-cooling driving crystal growth is sufficiently low that crystal shape is interface-controlled (Figure 3a). At low under-cooling (<1 to 5°C), the dominant growth mechanism for plagioclase is birth-and-spread (whereby crystal growth occurs by the sideways propagation of new layers across the pre-existing surface), with a sharp and well-defined melt-solid interface, and atomically smooth growing faces [*Kirkpatrick et al.*, 1976; *Cabane et al.*, 2005]. The plagioclase grains form networks at volume fractions as low as 25% [*Philpotts et al.*, 1998] by a combination of aggregation by synneusis (resulting in crystals lying parallel to each other [*Means and Park*, 1994]), and heterogeneous nucleation (resulting in crystals at high angles to each other [*Kirkpatrick*, 1981]). The resultant population of plagioclase-plagioclase-melt dihedral angles is widely distributed (high standard deviation) but with a median of order 60° (Figure 4a). This is the impingement microstructure described by *Elliott et al.* [1997] and *Holness et al.* [2005a].

[23] If the under-cooling is large, crystal growth becomes controlled by the rate at which new material can reach the melt-solid interface and a compositional boundary layer develops [*Kirkpatrick*, 1981]. This can destabilize the planar growth faces and result in the growth of elongate protuberances (Figure 3b). In the case of growth of a plagioclase framework diffusion control is most important close to the junctions of plagioclase grains, particularly if they meet at a low angle. *Holness et al.* [2005b] describes how this diffusion-limited growth results in curvature of the plagioclase-melt interfaces toward the junctions and the creation of low dihedral angles (Figure 3c). The population of these angles may become indistinguishable from that expected for plagioclase-melt textural equilibrium (Figure 4a) [*Holness et al.*, 2005b], although the distinction can otherwise be made from the presence of irregularities and protuberances on the interface (Figure 3c).

[24] The final case is one in which the temperature remains constant or changes very slowly, so the rate of growth does not exceed that of textural equilibration: grain shape and the geometry of grain junctions become controlled more by
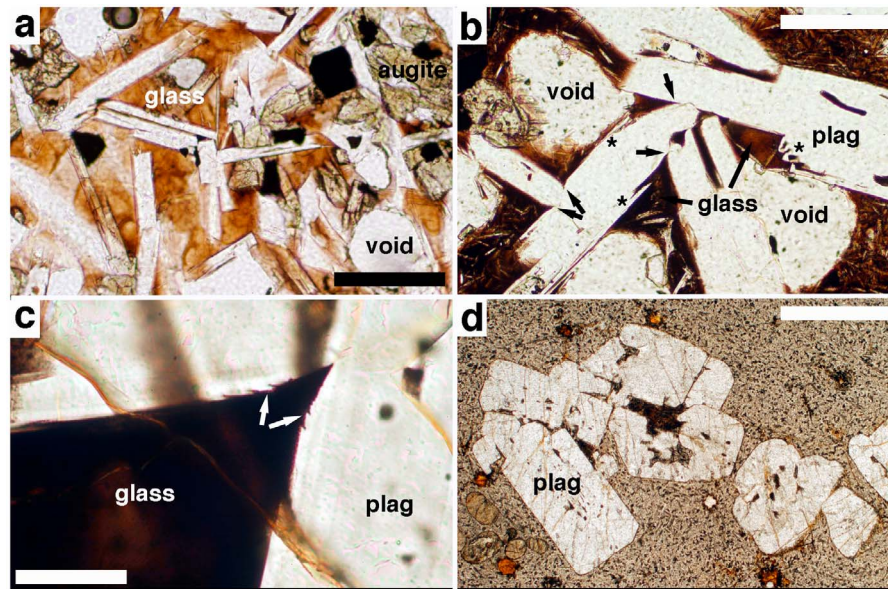
Figure 3. Microstructures in glassy plagioclase-bearing rocks. (a) Glassy nodule (sample K1–10) from Kameni. Note the random orientation of the impinging plagioclase grains and their generally planar-sided junctions. Scale bar is 200 μm long. (b) Glassy nodule (sample K0–5E) from Kameni with significant curvature at plagioclase-plagioclase junctions (arrowed) caused by diffusion-limited growth close to the junction itself. The asterisks mark elongate protuberances caused by diffusion-limited growth. Scale bar is 200 μm long. (c) Close-up of a junction from K0–5E showing serrations on the plagioclase-melt interface (arrowed) caused by breakdown of the planar growth face, indicative of diffusion-limited growth. Scale bar is 100 μm long. (d) Pitchstone, Beinn an Lochain, Mull (Harker Collection number 13485, University of Cambridge), with clots of rounded plagioclase set in a fine-grained matrix. The melt-plagioclase-plagioclase dihedral angles in this rock are in textural equilibrium [*Holness*, 2006]. Scale bar is 1 mm long.

interfacial energies than growth kinetics (Figure 3d). The plagioclase grains are rounded and equant, and melt-plagioclase-plagioclase dihedral angles are in textural equilibrium (a median of ~30° and a standard deviation of ~10°; Figure 4a) [*Holness*, 2006].

[25] The junction between two plagioclase grains and melt is therefore either formed by the meeting of two completely planar surfaces (if growth is not limited by diffusion), or the plagioclase-melt boundaries curve into the junction, forming a lower angle than would have been the case for planar faces (for diffusion-limited growth or textural equilibrium). A continuous progression between these two end-members (median of 60° and high standard deviation versus median of 30° and low standard deviation) has been observed in glassy amphibole-rich nodules and attributed to variable degrees of melt-solid textural equilibration [*Holness et al.*, 2005a], while a similar progression between the same end-member populations in plagioclase-rich enclaves has been ascribed to differing degrees of control on microstructure by diffusion-limited growth [*Holness et al.*, 2005b]: the distinction between these two very different situations is made on the basis of compositionally zoned overgrowths and protrusions on the erstwhile planar growth faces [*Holness et al.*, 2005b].

[26] In our experience, texturally equilibrated plagioclase-melt microstructures are rare. We have found no evidence for plagioclase-melt textural equilibrium preserved in fully solidified dolerites and gabbros: instead plagioclase grains are elongate in thin section, with planar growth faces. The plagioclase walls bounding glass-filled pockets in some

dolerites may be curved but this curvature is associated with irregularities indicative of diffusion-controlled growth (see later). Equilibrated crystal clots in lavas are rare [e.g., *Holness*, 2006].

[27] Details of the melt-plagioclase-plagioclase dihedral angle populations in glassy crystalline nodules from the Kameni Islands of Santorini [*Holness et al.*, 2005b] are reproduced here, with the addition of new data to give 70–100 individual measurements for each sample (Table 2). Many of the Kameni samples exhibit the irregular plag-melt interfaces and curved junctions indicative of significant diffusion-limited growth modification of the melt-plagioclase-plagioclase angles: the populations reported here are only for the unmodified angle measured far from the junction itself: these populations therefore reflect the angle between the {010} growth faces and, within error, have medians of 60°. The data form a trend on a plot of median versus standard deviation (Figure 4b) and *Holness et al.* [2005b] ascribed this to the propensity of the plagioclase crystals to form frameworks by heterogeneous nucleation. However, the 2σ errors on these median values are large (Table 2), and it is doubtful whether the trend has much significance.

4.2. Formation of a Plagioclase-Augite Poly-crystal

[28] Once the junction between two plagioclase grains has formed, pyroxene must then grow into the space between them. A qualitative understanding of this process can be gained from the upper solidification front of the Kilauea Iki
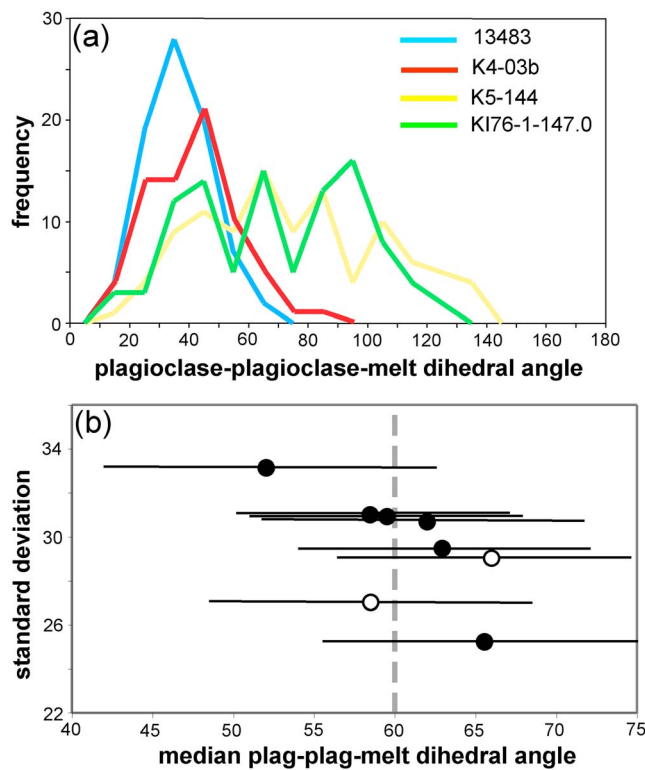
Figure 4. Dihedral angle populations for melt-plagioclase-plagioclase. (a) Frequency plots. K5–144 (glassy crystalline nodule entrained in the 1939 flow on Kameni) shows the distribution of angles between plagioclase grains far from the actual junction (i.e., ignoring the diffusion-controlled curvature at the junction itself; data from *Holness et al.* [2005b]). K4–03b (glassy crystalline nodule entrained in the 1940 flow on Kameni) shows the distribution of angles in a system with significant diffusion-limited growth leading to low dihedral angles (described in *Holness et al.* [2005b], whence the data come). Equilibrium plagioclase-plagioclase-melt angles from sample 13843 (Beinn an Lochain, Mull. Harker Collection number 13485, University of Cambridge [*Holness*, 2006]). This sample is shown in Figure 3d. KI76-1-147.0 shows the frequency distribution of plagioclase-plagioclase-melt angles in the partially solidified zone of the Kilauea Iki lava lake, measured at the junction itself. See Table 3 and the text for more details about this sample. These four samples provide an indication of the probable range of melt-plagioclase-plagioclase angles in natural systems. (b) The median and standard deviation of melt-plagioclase-plagioclase junctions. Black dots: data for glassy crystalline nodules from Kameni, measured far from the actual junctions, with the 95% confidence intervals shown (see Table 2 for details). White circles: data for melt-plagioclase-plagioclase junctions measured at the actual junctions in partially crystalline samples from Kilauea Iki lava lake (see Table 3 for details). The dashed line at 60° gives the expected median value for a true impingement texture in which the plagioclase grains are randomly oriented.

lava lake. This lava lake was filled in late 1959 and early 1960 by olivine-phyric basalt [*Richter et al.*, 1970].

[29] The suite of samples from the 1976 drill hole [*Helz et al.*, 1984] examined for this study range from the lowermost sample in the hole (with 36 vol.% glass, quenched from 1106°C) [*Helz and Thornber*, 1987] to several samples collected from the fully solidified crust (with 13 vol.% glassy mesostasis). The shallowest sample from this borehole is thought to have been sub-solidus since 1972. The mineral modes and dihedral angle data are presented in Table 3, together with estimates of their quench temperature (reported in *Helz and Thornber* [1987]) determined from glass MgO content (samples from 45.42–43.68 m depth) or from glass CaO content (42.76 m depth) The temperature in the sample from 41.15 m depth is estimated by extrapolation from greater depths. The increase in olivine mode with increasing depth in the core is caused by crystal settling [*Helz*, 1987, 2009].

[30] The hottest samples from this drill core comprise chains of elongate plagioclase grains with a separate interlocked set of clusters of equant, facetted augite grains (Figures 5a–5c). The average grain size of the augite is generally of the order of the average thickness of the plagioclase laths (Figures 5a and 5b). There are comparatively few intraphase grain boundaries and very few intraphase three-grain junctions. The melt-plagioclase-plagioclase junctions are planar-sided, with no evidence for either diffusion-limited growth in the pore corners or textural equilibration (Figures 5c, 5g, and 5h). The melt-plagioclase-plagioclase angles were measured in the two lowermost samples (Table 3) and are similar to the unmodified populations measured in the Kameni nodules (Figure 4). This is consistent with crystal growth at low undercoolings and a rapid quench during the drilling. Ilmenite forms isolated elongate blades (Figure 5a), some with dendritic habit. The olivine crystals are the focus of (heterogeneous) nucleation and growth of plagioclase and augite (Figures 5d–5f): this means that the volume fraction of glass is always lower in the immediate vicinity of the olivine phenocrysts (Figure 5e). As crystallization proceeds the average grain size of the plagioclase and augite in the rims surrounding the olivine phenocrysts remains lower than that far from the phenocrysts (Figure 5f), due to the earlier impingement of the closely spaced crystals in the rim.

[31] As soon as plagioclase and augite grow close enough, the attraction resulting from a nonzero augite-plagioclase-melt dihedral angle (i.e., $\gamma_{gb} < 2 \gamma_{sl}$) [*Rappaz et al.*, 2003] means that they will form a grain boundary. This begins to be important at 44.29 m depth (i.e., about 1 m from the

Table 2. Plagioclase-Plagioclase-Glass Dihedral Angles in Glassy Crystalline Nodules Entrained in the Recent Lavas From the Kameni Islands, Santorini[a]

Sample	n	Median[b]	Standard Deviation	Skew
K6–21	100	58.5 ± 8	31.01	0.5
K5–144	100	62 ± 10	30.71	0.3
K3–255	100	52 ± 10.5	33.17	0.4
K5–285	72	59.5 ± 8.5	30.92	0.6
K4–06	70	63 ± 10	29.50	0.3
K4–01	70	65.5 ± 9.5	25.28	−0.4

[a]The angles were measured far from the plagioclase-plagioclase junctions to avoid the effects of diffusion-limited growth in the pore corners. Some of these data have previously been reported by *Holness et al.* [2005b].
[b]The errors give the 95% confidence interval calculated according to *Stickels and Hücke* [1964].

Table 3. Mineral Modes and Dihedral Angle Data for Samples From the Kilauea Iki Lava Lake, Drilled in 1976

Sample	Depth in Core (m)	Quench Temperature[a] (°C)	Vol.% Ol[b]	Vol.% Cpx	Vol.% Plag	Vol.% Glass	Vol.% Oxide	Vol.% Void	Cpx-Plag-Plag				Glass-Plag-Plag			
									n[c]	Median[d] (Θ_{cpp})	Standard Deviation	Skew	n	Median	Standard Deviation	Skew
KI76-1-110.5	33.68	-	-	-	-	-	-	-	100	78.5 ± 3.5	18.42	-0.2	-	-	-	-
KI76-1-123.4	37.61	-	-	-	-	-	-	-	100	79 ± 3.5	16.72	0.2	-	-	-	-
KI76-1-135.0	41.15	~985	3.0	39.1	39.6	12.7	5.2	0.4	50	84.5 ± 4.5	19.12	-0.3	-	-	-	-
KI76-1-140.3	42.76	1011	7.9	37.0	32.4	15.3	6.1	1.3	50	92 ± 5	12.51	-1.2	-	-	-	-
KI76-1-143.3	43.68	1058	2.7	33.9	35.3	22.3	4.0	1.5	50	96 ± 3.5	13.63	-0.5	-	-	-	-
KI76-1-145.3	44.29	1073	6.9	34.1	28.5	25.6	2.8	1.7	50	97.5 ± 5.5	13.40	-0.8	-	-	-	-
KI76-1-147.0	44.81	1087	11.7	25.6	27.2	30.6	2.5	2.0	40	100 ± 5.5	13.18	-0.6	100	58.5 ± 10	27.23	0.0
KI76-1-149.0	45.42	1106	15.9	23.2	21.0	35.7	0.1	3.8	30	102 ± 3.5	13.35	-0.4	100	66.5 ± 9	29.17	-0.1

[a]From *Helz and Thornber* [1987].
[b]The modes were determined by point counting 1000 points per sample.
[c]The number of individual measurements in each dihedral angle population.
[d]The error on the median is the 95% confidence interval calculated according to *Stickels and Hücke* [1964].

lowest drillable part of the solidification front) where the individual chains and clusters of the plagioclase and pyroxene (augite is joined by pigeonite once the temperature drops below ~1090°C) start to form appreciable numbers of intraphase grain boundaries and three-grain junctions. At 42.76 m depth (~2.5 m from the lowest drillable part of the solidification front), small ilmenite grains nucleate on the surfaces of pyroxene crystals (Figures 5g and 5j). Ilmenite

otherwise forms good grain boundaries with plagioclase (Figure 5a). The samples from the fully solidified crust of the lava lake contain abundant pockets filled with glass and fine-grained late-stage evolved assemblages (Figures 5g and 5h).

[32] Pyroxene does not always penetrate into the pore corner: some plagioclase-plagioclase junctions contain small pockets of glass, bounded by a curved pyroxene surface (this
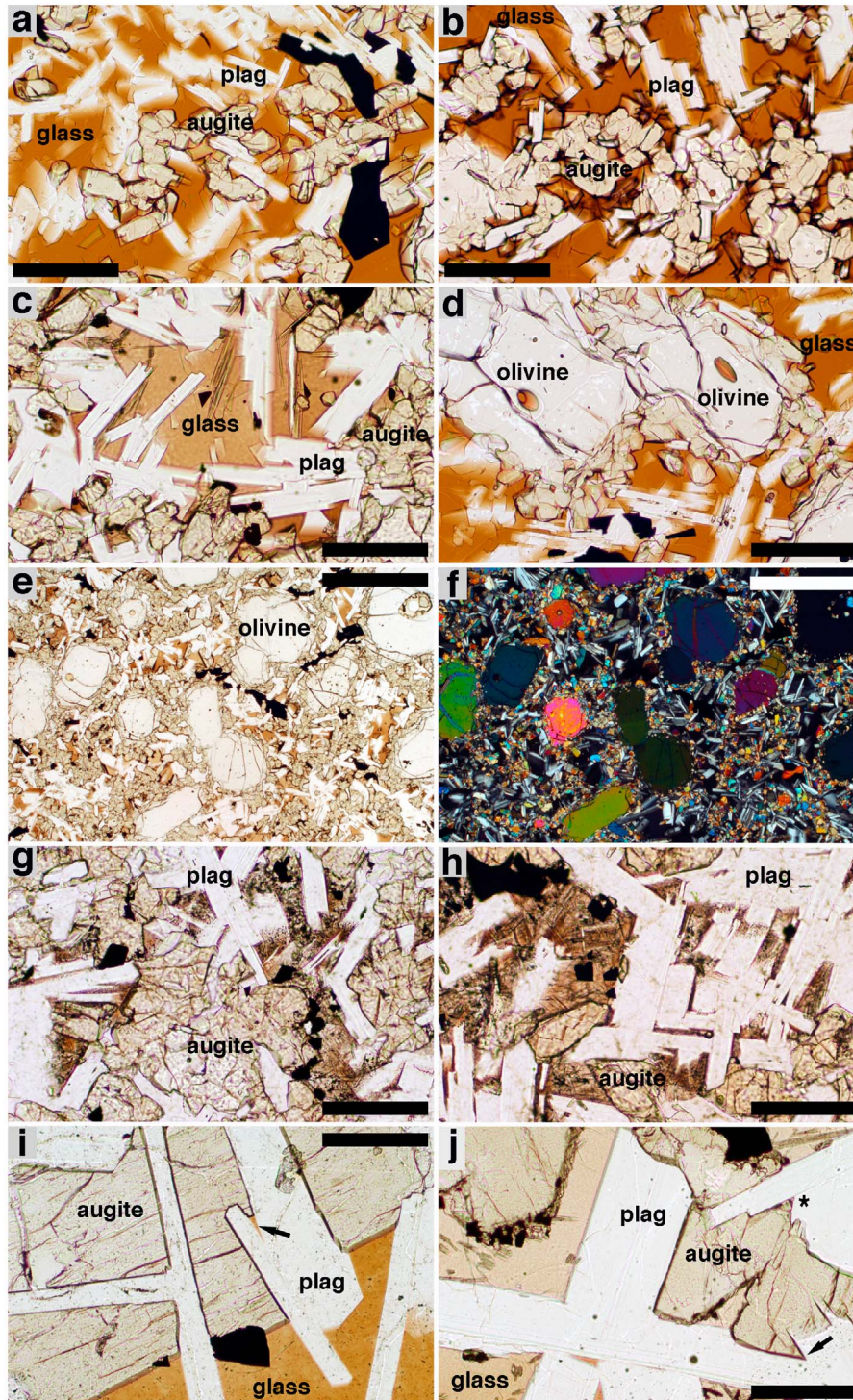

Figure 5

is illustrated in Figures 5i and 5j which show the feature in relatively coarse-grained segregation veins). This is most noticeable for junctions where the two plagioclase grains meet at a low angle. The fully formed (i.e., glass-absent) three-grain junctions are formed either by perfectly planar plagioclase-pyroxene boundaries (parallel to a growth face of the plagioclase) or by boundaries with a slight curvature, forming a higher angle than would have been the case for planar faces (Figures 5i and 5j). Lower angles (i.e., curving to a sharper, rather than a blunter, point) are rare.

[33] We measured the cpx-plag-plag dihedral angles, taking particular care to avoid those with a residual glass pocket. 100 individual measurements were made in samples with abundant intraphase three-grain junctions. Samples from deep in the core contain very few fully formed triple junctions and only 30 measurements could be made on the single thin section of the hottest sample (Table 3). The medians of these populations, denoted Θ_{cpp}, decrease from a maximum of 102° toward a final value of ~78° in the fully solidified crust. The standard deviations of the glass-rich samples are relatively low but this may be an artifact of the small populations [Holness, 2010].

[34] These data show that the progressive formation of a population of pyroxene-plag-plag junctions occurs by the preferential early infilling of the widest melt-plag-plag junctions, leading to a high initial median (Figure 6). As solidification proceeds augite (and pigeonite, once it becomes a volumetrically important component of the crystallizing assemblage) begins to infill pores bounded by plagioclase grain intersecting at lower angles. All possible pyroxene-plag-plag junctions are formed when the basalt has crystallized by about 88–90 vol% (Table 3 and Figure 6) - the remaining liquid-filled pockets quench to a mixture of silica-rich glass and dendritic grains.

4.3. Dihedral Angle Variation in Dolerites

[35] We now extend investigation to bodies that solidified over a longer period than the ~10 years taken by lava lakes. We chose two bodies for comparison: the rapidly cooled Traigh Bhàn na Sgùrra sill on the Isle of Mull (Scotland) to provide a link between the lava lake (with a comparable

cooling rate) and fully solidified dolerites, and the relatively slowly cooled Portal Peak sill of Antarctica.

[36] The Traigh Bhàn na Sgùrra dolerite sill is part of the Tertiary Loch Scridain Sill Complex, intruded into Precambrian Moine schists. It outcrops over several kilometers and has a thickness ranging from 2.5 m to >10 m although for most of its outcrop it is ~3 m thick. Variable contact metamorphism of its walls provides evidence of flow localization in the sill, with some parts acting as long-lived conduits for magma [Wartho et al., 2001; Holness and Humphreys, 2003]. The sill is composed of olivine-poor or olivine-free tholeiitic dolerite, with elongate plagioclase grains surrounded by ophitic augite (Figure 7a). Phenocrysts of plagioclase are rare. Between the grains of plagioclase, augite and rare olivine are pockets of silica-rich mesostasis comprising brown altered glass containing dendritic crystals (Figures 7b–7d).

[37] We measured Θ_{cpp} for four samples from the sill, two from the center of the long-lived parts (ROM48–219 and ROM43–170) and two from the margin (ROM43–35 and ROM43–80) (i.e., including samples covering the full range of cooling rates). We also measured the angle subtended at the corners of mesostasis-filled pockets for comparison with those filled with clinopyroxene (Figure 7b). The results are given in Table 4 and shown in Figure 8. The four Traigh Bhàn na Sgùrra samples have similar values of Θ_{cpp} and standard deviation: these angle populations resemble those in the uppermost two samples from the crust of the lava lake (Table 3 and Figure 8). However, the mesostasis-plag-plag dihedral angle populations have much lower medians (as low as 42.5°) and higher standard deviations, with positive skew. The Traigh Bhàn na Sgùrra plagioclase-mesostasis and plagioclase-pyroxene dihedral angle populations fall on either side of the cloud of (impingement) data points collected from the Kameni nodules and the lowermost two samples of the lava lake solidification front (Figure 8). There is no apparent relationship between Θ_{cpp} in the Traigh Bhàn na Sgùrra samples and the associated median of the melt-plagioclase-plagioclase population within the uncertainties of the data.

Figure 5. Photomicrographs showing details of the microstructures developed during progressive solidification of the Kilauea Iki lava lake. (a) KI76-1-147.0 (44.81 m below the lake surface). Note the elongate cluster of equant augite crystals (pale brown) crossing the middle of the image, together with the interlocking framework of plagioclase laths (colorless) sitting in a matrix of glass (mid-brown). Ilmenite (black) readily forms inter-phase grain boundaries with plagioclase. Scale bar is 200 μm long. (b) KI76-1-149.0 (45.42 m depth). Augite and plagioclase form clearly separate clusters, suggestive of heterogeneous nucleation. Scale bar is 200 μm long. (c) KI76-1-140.3 (42.76 m depth). Note the planar-sided plagioclase grains, with no curvature of the plagioclase-melt interfaces where they intersect. Augite crystals form separate clusters. Scale bar is 200 μm long. (d) KI76-1-147.0 (44.81 m depth). Olivine phenocrysts are mantled by plagioclase and augite, suggestive of heterogeneous nucleation. Scale bar is 200 μm long. (e and f) KI76-1-140.3 (42.76 m depth) Glass (mid-brown) is concentrated in pockets between olivine phenocrysts which are mantled by low porosity plagioclase and augite aggregates. Scale bar is 1 mm long. Under crossed polars (Figure 5f) it is clear that these early formed rims are fine-grained relative to the plagioclase and augite between the phenocrysts. (g and h) KI-1-123.4 (37.61 m depth). Scale bars in both images are 200 μm long. This sample comes from the fully solidified (albeit glass-bearing) crust of the lake. Note the abundance of planar-sided pockets of glassy mesostasis (mid-brown) containing fine dendritic grains. The glass-plagioclase-plagioclase junctions are planar-sided. (i) KI76-1-143.3 (43.68 m depth). Segregation vein. Note the straight plagioclase-augite junctions defined by the growth faces of the plagioclase. Some three-grain junctions are formed of planar intersections, while a small glass-filled pocket (arrowed) remains where two plagioclase grains intersect at low angle. Scale bar is 200 μm long. (j) KI76-1-140.3 (42.76 m depth). Segregation vein. Note the ilmenite grains (black) nucleating on augite-melt interfaces and the planar intersections at three-grain junctions (arrowed). Others are partially formed and contain a small glass pocket (denoted by *). Scale bar is 200 μm long.
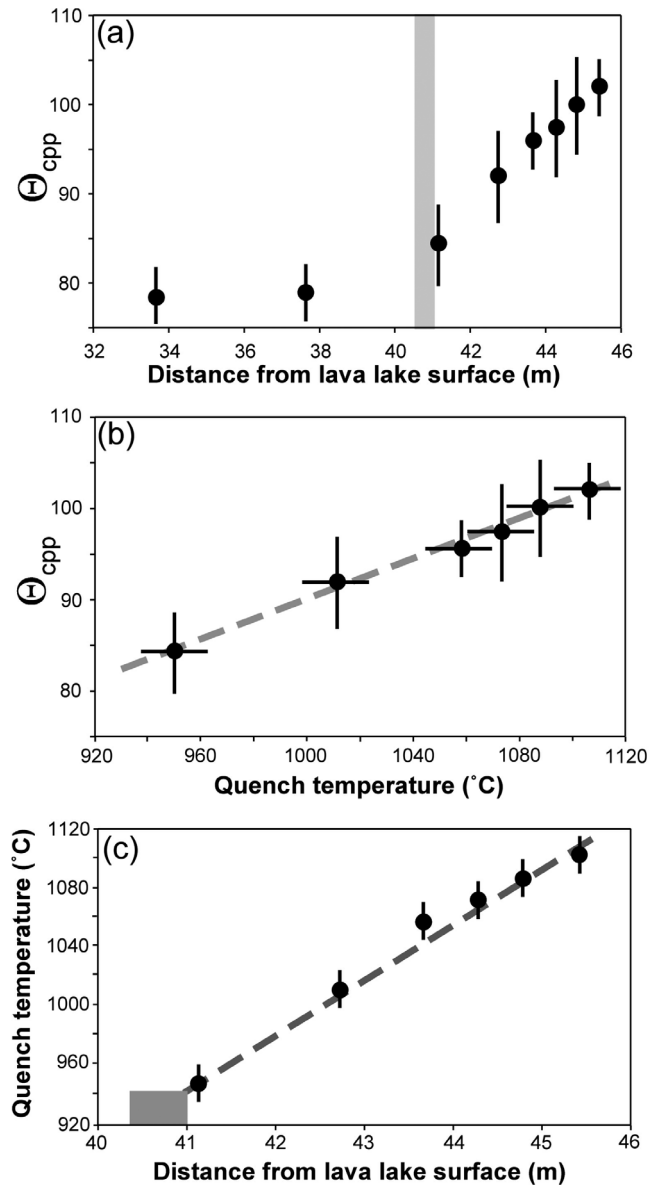
Figure 6. Microstructural variation in the upper solidification front of the Kilauea Iki lava lake sampled by the 1976 drill hole. (a) Median cpx-plag-plag dihedral angle as a function of depth in the core. The error bars for the median values give the 95% confidence interval. The gray bar gives the approximate position of the solidification front. (b) The variation of median dihedral angle as a function of quench temperature in the six samples below the base of the solid crust at ∼41 m depth, determined from the composition of glass [*Helz and Thornber*, 1987]. The line of best fit was estimated by eye. (c) The variation of calculated quench temperature as a function of depth in the core. The line of best fit was estimated by eye. The gray shaded area shows the estimated depth and temperature range of the base of the solid crust. The width is the best estimate of the position of the base (from Figure 6a), while the height of the shaded area is taken from the slope of the line of best fit in Figure 6c).

[38] The ∼130 m thick Portal Peak sill is part of the Ferrar group of sills, and intrudes metasediments of the Beacon Supergroup at 83°50′S, 165°36′E, near the Beardmore Glacier in the Transantarctic Mountains [*Faure and Mensing*, 2010]. The tholeiites are fine-grained to glassy near the chilled contacts and coarsen into the interior of the sill. The main phases are plagioclase, augite and pigeonite, with a mesostasis that commonly comprises a granophyric intergrowth of quartz and feldspar (Figure 7e). Dihedral angles are commonly formed of planar plagioclase-augite grain boundaries (Figure 7f) but toward the center of the sill there is noticeable curvature at the junctions, with the boundaries curving to make higher angles than those predicted by extrapolating the augite-plagioclase boundaries far from the junction (Figures 7g and 7h).

[39] We measured Θ_{cpp} in the center of the sill (samples 87–101 and 87–110) and on the margins (samples 87–89 and 87–124), and the results are presented in Table 4. The margins of the Portal Peak sill have dihedral angle populations indistinguishable from those of the Traigh Bhàn na Sgùrra sill and the solidified crust of the lava lake (Table 3), while Θ_{cpp} at the sill center is significantly higher and with a lower standard deviation, falling on a linear trend toward the equilibrium population on a plot of Θ_{cpp} vs standard deviation (Figure 8).

4.4. Controls on Primary Dihedral Angle Formation During the Igneous Process

[40] Earlier studies were based on the assumption that the initial cpx-plag-plag angle population is essentially the same as that of the immediately preceding melt-plag-plag population (Table 2 and Figure 4). For the lava lakes, and by inference for all dolerites, this would result in Θ_{cpp} of ∼60°. However, Θ_{cpp} in both the fully solidified (although not fully crystalline) lava lake crust and at the margins of the two dolerite sills we have investigated, is ∼78°. It is a reasonable proposition that the microstructure in these examples reflects that immediately subsequent to solidification and is thus primary. Because the median dihedral angle is significantly higher than the median melt-plag-plag angle of 60° the initial cpx-plag-plag angle population cannot be created by pseudomorphing of the melt-filled porosity. Instead, augite preferentially fills the wider pores. Pockets containing glass (i.e., those that did not fully crystallize) tend to be those where plagioclase grains meet at a low angle (Figures 7b, 7d, and 8); this explains why the Traigh Bhàn na Sgùrra sill melt-bearing angles are all <60°. Pore size is clearly important in determining primary solidification microstructures.

4.4.1. The Importance of Pore Size

[41] It is well known that solid particles with curved surfaces in contact with a liquid require a more concentrated solution to remain in equilibrium compared to the same material with a flat surface in contact with the same liquid. The relationship between radius of curvature and the undercooling required for further crystal growth is described by the Ostwald-Freundlich equation:

$$\frac{2\gamma}{r} = \frac{RT}{V} \ln\left(\frac{C}{C_o}\right)$$
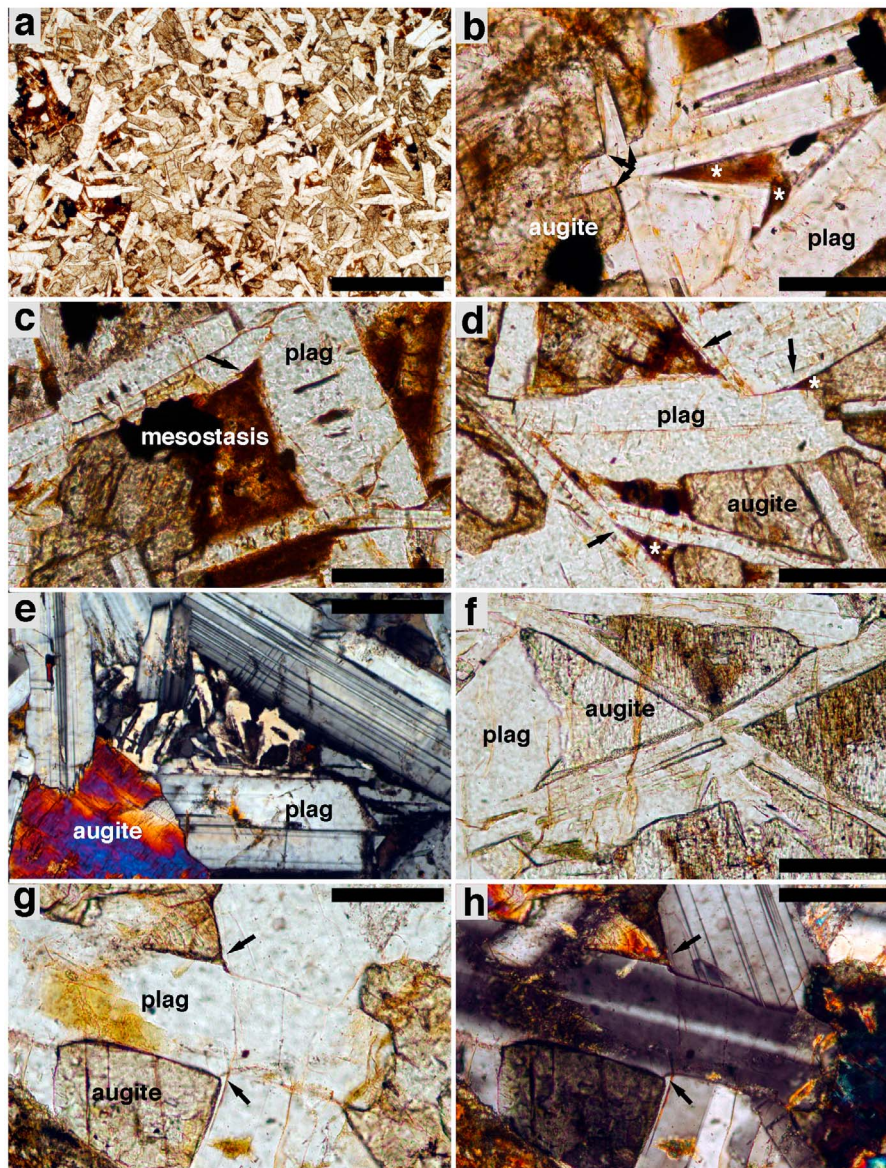
Figure 7. Photomicrographs of dolerite sills. (a–d) ROM48–219 from the center of the Traigh Bhàn na Sgùrra sill where it is 3.5 m thick and flow was continuous over a period of months. In Figure 7a the microstructure comprises randomly oriented plagioclase laths with interstitial augite and rare olivine. Scale bar is 1 mm long. In Figure 7b augite fills the wider plagioclase-plagioclase junctions (arrowed) in preference to the narrower junctions (now filled with mesostasis, marked by an asterisk: similar mesostasis-filled, narrow, junctions are also denoted by an asterisk in Figure 7d). Scale bar is 100 μm long. In Figure 7c some mesostasis-plag junctions are curved: the compositional zoning on the margins of the plagioclase grains, together with irregularities of the interfaces (see also Figure 7d), is consistent with diffusion-limited growth. Scale bar is 100 μm long in both Figures 7c and 7d. (e) Sample 87–101 from the center of the Portal Peak sill. Pockets of late-stage silicic material crystallized as granophyre instead of the glassy mesostasis of the more rapidly cooled Traigh Bhàn na Sgùrra sill. Scale bar is 200 μm long. (f) Sample 87–89 from the margin of the Portal Peak sill. Note the angular cpx-plag-plag junctions formed by the intersection of planar plagioclase-augite grain boundaries. Scale bar is 200 μm long. (g) Sample 87–106 from the center of the Portal Peak sill, shown in plane polarized light, with the same field of view under crossed polars shown in Figure 7h. (h) Three-grain junctions are now commonly rounded (arrowed), with compositional zoning of the plagioclase demonstrating that this geometry is a primary igneous feature. Scale bar is 200 μm long.

Table 4. Dihedral Angle Data for the Traigh Bhàn na Sgùrra and Portal Peak Sills

| Sample | \(n\) | Cpx-Plag-Plag Angles | | | \(n\) | Mesostasis-Plag-Plag Angles | | |
		Median (\(\Theta_{cpp}\))	Standard Deviation	Skew		Median	Standard Deviation	Skew
			Traigh Bhàn na Sgùrra					
ROM48–219	60	78.5 ± 4.5	19.4	−0.9	100	58.5 ± 11.5	30.2	0.5
ROM43–35	100	78.5 ± 4.5	23.1	−0.5	100	49.5 ± 12	28.2	0.3
ROM43–80	104	78.5 ± 5.5	20.5	−0.3	100	43 ± 6.5	26.4	0.7
ROM43–170	100	85 ± 4	20.4	−0.9	100	42.5 ± 7	27.4	0.6
			Portal Peak					
87–89	100	79.5 ± 3.5	21.9	−0.3	-	-	-	-
87–124	100	78.5 ± 5	21.3	−0.7	-	-	-	-
87–101	100	94 ± 3.5	14.8	−0.3	-	-	-	-
87–110	100	94.5 ± 3.5	15.0	−1.7	-	-	-	-

where γ is the melt-solid interfacial energy, r is the radius of curvature of the melt-solid interface, R is the gas constant, T is temperature, V is the molar volume of the solid, C is the concentration of the liquid in equilibrium with the crystal of radius r, and C_o is the concentration in equilibrium with a planar melt-solid interface [*Cahn*, 1980; *Adamson*, 1990]. This relationship leads to Ostwald ripening in polydisperse materials, whereby large particles grow at the expense of smaller particles [*Ostwald*, 1901]. The same relationship applies to nucleation in fluid-filled pores: the smaller the pore, the greater the supersaturation required in order to nucleate a crystal within it [e.g., *Bigg*, 1953; *Melia and Moffitt*, 1964; *Cahn*, 1980; *Scherer*, 1999; *Putnis and Mauthe*, 2001; *Cesare et al.*, 2009].

[42] This means that the thermodynamics of crystallization in small pores is different from that in a free fluid: most importantly, for a given rate of cooling a confined fluid can become more supersaturated before crystallization begins compared to an unconfined fluid of the same composition [e.g., *Bigg*, 1953; *Melia and Moffitt*, 1964; *Cahn*, 1980; *Scherer*, 1999; *Putnis and Mauthe*, 2001]. Crystallization in a liquid-bearing rock with a range of pore sizes will therefore occur over a range of temperature: nucleation and growth will begin first in the largest pores, but will be delayed (or even prevented) in the smallest [*Cesare et al.*, 2009]. This can be demonstrated by examination of lava flows containing phenocrysts with glassy melt inclusions or glassy

crystalline nodules. A typical example is a glass-bearing, crystal-rich, gabbroic nodule from the basaltic Borgahraun flow from the Theistareykir segment of the Northern Volcanic Zone of Iceland [*Maclennan et al.*, 2003], dominated by plagioclase and clinopyroxene. The plagioclase is blocky and equant and contains numerous melt inclusions of variable sizes and crystallinity (Figure 9). The smallest inclusions are elongate, with planar sides and rounded ends. The shape of the largest inclusions is highly irregular.

[43] The crystallinity of the plagioclase-hosted melt inclusions can be estimated from backscatter images of polished samples: each inclusion can be categorized as either glassy, finely crystalline, or coarsely crystalline. The apparent short axis of each inclusion was measured with an accuracy of a few microns. The average width of tapered inclusions was taken to be the short axis, while a visual estimate was made of the average dimension of the largest irregular inclusions. Fifty examples were chosen of each of the three main categories. The melt inclusions show a clear pattern of increasing crystallinity with melt inclusion size (Figure 9). The smallest inclusions (1–6 μm on the short axis) are glassy, while the largest are coarsely crystalline. A coarsely crystalline texture is observed in melt inclusions with a short axis of >10 μm, while those of intermediate size are finely crystalline. The cut-off between glassy and finely crystalline microstructures occurs for inclusions in the 7–10 μm size range. Note that these dimensions are necessarily approximate due to the
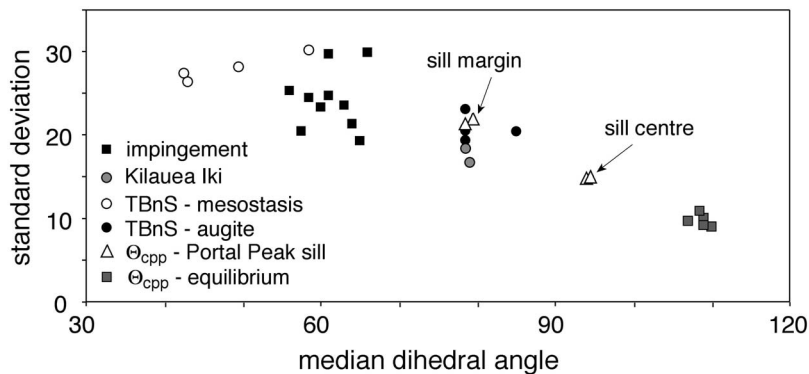
Figure 8. Median dihedral angle versus standard deviation, showing the range of data for plagioclase impingement microstructures (from Kameni nodules and the lowermost two samples from the Kilauea Iki crust (Tables 2 and 3)), Θ_{cpp} from the uppermost two samples of the Kilauea Iki crust (Table 3), mesostasis-plag-plag (or glass-plag-plag) and Θ_{cpp} from the Traigh Bhàn na Sgùrra sill (Table 4), Θ_{cpp} from the Portal Peak sill (Table 4) and equilibrium Θ_{cpp} (Table 1).
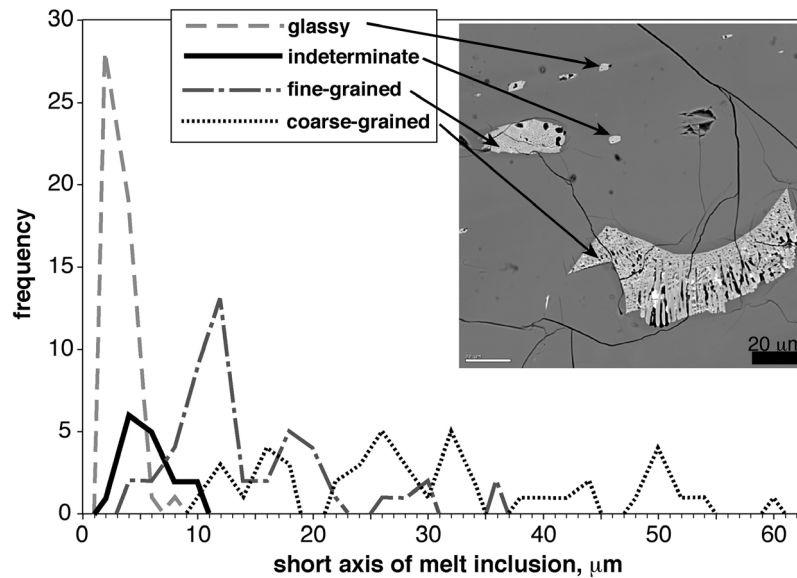
Figure 9. Melt inclusions in plagioclase phenocrysts from the Borgahraun flow from the Theistareykir segment of the Northern Volcanic Zone of Iceland range from glassy, through finely crystalline to coarsely crystalline (inset backscatter electron image). The extent of crystallinity of each inclusion shows a strong correlation with its apparent short axis measured in a single polished thin section. The coarsely crystalline inclusions are large, while the glassy inclusions are all <10 microns across. Those inclusions for which the resolution on the scanning electron microscope was insufficient to decide whether they were glassy or crystalline fall in a narrow size range denoted by the heavy line on the frequency plot.

effects of random 2-D slicing through 3-D objects. These effects are most likely to be important for the largest and most irregular of the inclusions.

[44] The example provided by melt inclusions concerns crystallization in entirely closed fluid pockets. Solidification of small, interconnected fluid pockets in a polycrystal may additionally be affected by a reduction in mass transport (by either diffusion or porous flow) during progressive solidification. As pores get smaller, the permeability of the pore network is reduced, making it more likely that crystal growth will result in a depletion of the adjacent liquid in essential components required for further growth (c.f. Figures 3c and 7c). *Holness and Sawyer* [2008] showed that the composition of plagioclase grains growing in melt-filled pores becomes more albitic in the narrower parts of the pores. While this might be entirely due to surface energy effects (with the reduction in radius of curvature accompanying growth into the narrower parts of the pore leading to a greater undercooling required for growth), it is also possible that a similar effect might be caused by difficulties in mass transport in the narrowest pores.

[45] The magnitude of the effects of pore size on crystallization temperature is illustrated by partially melted gneisses. The sample KR03/1 is a quartzo-feldspathic biotite gneiss from the aureole of the Skaergaard Intrusion (see *Kays et al.* [1989] for rock descriptions). It was collected from $68°10'33.3''N$ and $31°46'7.0''W$, a few centimeters from the contact with the intrusion. It contains large, restitic sieve-textured grains of plagioclase and K-feldspar set in a granophyric groundmass. The sites of original large biotite grains are marked by aggregates of orthopyroxene and ilmenite, together with small, randomly oriented grains of new biotite, enclosed by K-feldspar. The pores within the sieve-textured feldspar grains are filled with quartz, forming optically continuous crystals up to 300 microns across (Figure 10, top).

[46] The titanium content of quartz was determined using wavelength dispersive electron microprobe spectrometry at the Department of Earth Sciences, University of Cambridge (see Appendix A for operating conditions). The Ti contents were converted to quartz crystallization temperature using the TitaniQ thermometer of *Wark and Watson* [2006]. Since rutile is absent in this rock, calculated temperatures are minimum estimates although the relative differences are accurate if TiO_2 activity remained constant during crystallization [*Wark and Watson*, 2006].

[47] The width of the quartz pockets in the sieve-textured plagioclase was measured for each analysis, while in the granophyre the shortest distance across any quartz grain was measured. These distances are plotted against Ti content in Figure 10 (bottom). The Ti content of the quartz correlates with quartz dimensions: the highest values are found in quartz grains larger than about 30 μm across (450–750 ppm), while the lowest values (down to 200 ppm) are found in the smallest grains. There is commonly a decrease in Ti content along any one quartz grain in a granophyric intergrowth from the widest to the narrowest end. The difference in inferred crystallization temperature between the most Ti-rich and least Ti-rich quartz grains is of the order 150°C. These data demonstrate that the effects of pore size on crystallization (due to the effects of a reduced radius of curvature and/or diffusion-limited growth at low permeabilities) can be extremely important once the pore size decreases below a critical minimum. For both the gneiss described here and that described in *Holness and Sawyer* [2008] this minimum is of order 100 μm (Figure 10).
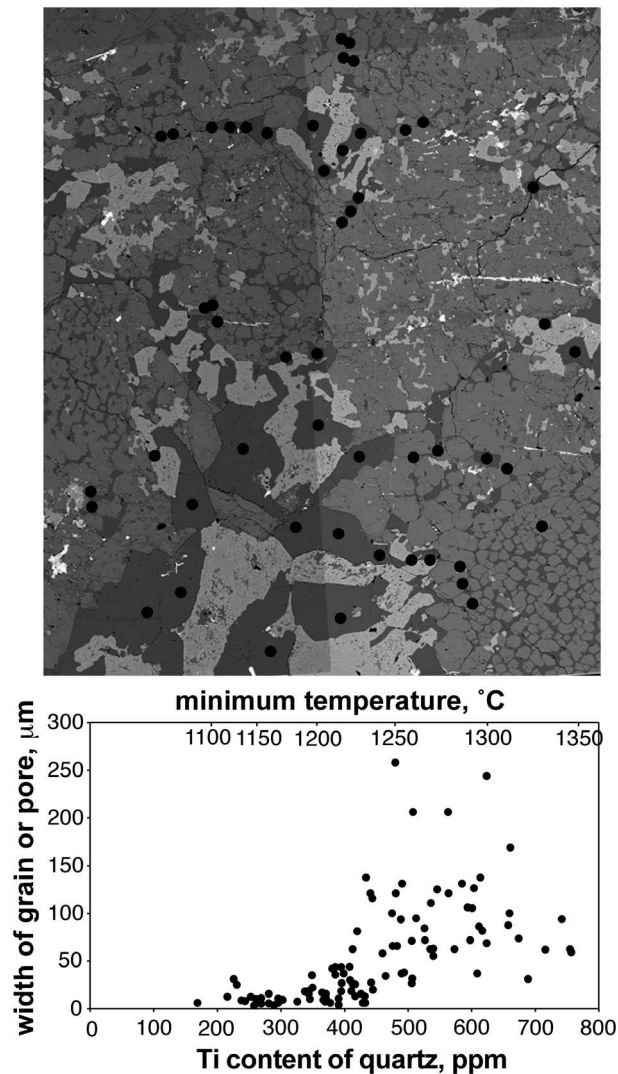
Figure 10. The effect of pore size on crystallization temperature in a partially melted quartzo-feldspathic gneiss, western margin of the Skaergaard intrusion, East Greenland. (top) Backscatter electron microscope image of the sample, with dots showing the position of representative analysis spots. (bottom) The Ti content of the quartz as a function of pore width (in the sieve-textured feldspar) and quartz grain diameter (in the granophyric pockets). These Ti contents are converted to temperature (upper scale) using the TitaniQ thermometer [*Wark and Watson*, 2006].

[48] It is possible that a higher cooling rate than that of the lava lake or the Traigh Bhàn na Sgùrra sill could create sufficient undercooling to drive the augite into the narrowest pores (resulting in a lower Θ_{cpp}), but these rapid cooling rates would mean both that mass transport might become limiting and that the glass transition temperature would be higher. Further work needs to be done decoding the balance of these two processes as a function of cooling rate in rapidly cooled rocks.

4.4.2. The Importance of Cooling Rate

[49] While Θ_{cpp} in rapidly cooled bodies is higher than 78° due to the preference for augite to grow in wider pores, there is a further effect resulting in generally higher angles than that expected for a perfect pseudomorphing of the plagioclase-melt geometry. Perfect pseudomorphing is indicated by cpx-plag-plag junctions formed by the intersection of two *planar* plagioclase-pyroxene grain boundaries: this points to the growth of pyroxene into a pore without accompanying growth of the pore walls [*Holness*, 2010] (Figures 11a and 11c). However, junctions with localized curvature (Figures 2, 7g, and 7h) must be formed by simultaneous growth of pyroxene *and* plagioclase (Figures 11b and 11d). The extent of simultaneous growth appears to be controlled by cooling rate, with more grain boundary curvature (and thus higher Θ_{cpp}) seen in the center of the Portal Peak sill compared to the sill margin. Fast cooling results in rapid pyroxene growth into the pore and insignificant growth of the plagioclase pore walls (low Θ_{cpp}), while slow cooling results in more commensurate pyroxene and plagioclase growth rates – the remaining melt pocket at the three-grain junction is filled with both plagioclase and pyroxene (high Θ_{cpp}).

[50] There are a number of possible controls on the relative rates of growth of different minerals. The plagioclase-melt interfaces bounding the pore are planar and are most likely to grow by a birth-and-spread mechanism. At low under-coolings, augite grows predominantly by spiral growth on screw dislocations [*Kirkpatrick et al.*, 1976], leading to much faster growth rates compared to birth-and-spread [*Gilmer*, 1976]: at low undercooling augite will therefore grow faster than plagioclase. Additionally, the augite-melt interface is not always planar: curved interfaces suggest an atomically rough surface, with growth by continuous mechanisms [*Kirkpatrick*, 1975]. This would also result in faster growth of curved augite crystals compared to planar-sided plagioclase as there is no need to nucleate a new surface layer.

[51] Since plagioclase and augite grow with different interface-controlled mechanisms, their response to changing under-cooling is different. At very low under-coolings, growth on screw dislocations is faster than growth by surface nucleation. As the undercooling increases, the advantage enjoyed by augite is eroded and surface-nucleation growth of plagioclase becomes faster. At any given position in an intrusion the under-cooling increases with increasing crystallization. Therefore, ignoring the problems posed by confinement in small pores (and ignoring any effects of changing liquid and solid composition), as crystallization proceeds one might expect a loss of dominance of augite growth and the emergence of significant plagioclase growth. This might lead to a transition between the early stages of crystallization during which augite fills up melt-filled pores relatively fast, to one in which augite growth slows and plagioclase growth begins to be important – this crossover may account for the morphology of most of the junctions in the center of Portal Peak in which augite-plagioclase boundaries are planar until right at the junction itself where there is evidence for infilling of the last space by plagioclase (Figure 7h).

[52] On an intrusion-wide scale, the under-cooling decreases with distance from the margin for a given fraction crystallized [*Kirkpatrick*, 1976]. This might suggest relatively rapid augite growth in the sill center resulting in low Θ_{cpp}, the converse to what is actually observed. However, it is possible that the high under-coolings generated in small bodies (and at the margins of larger bodies) create the
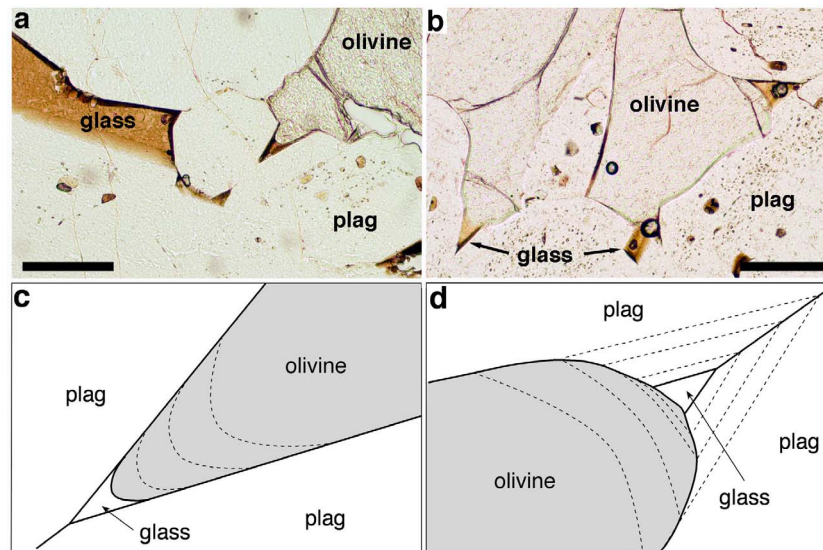
Figure 11. The effects of changing the relative growth rates of the two phases on the final geometry of the three-grain junction. Figures 11a and 11b show glassy olivine gabbro nodules entrained in a lava flow, Iceland, illustrating the details of melt pockets partially infilled by olivine [from *Holness*, 2010]. Scale bars in both images are 200 μm long. These rocks were quenched rapidly on entrainment in the magma: the presence of glass thus reflects the entrainment process and not the cooling rate experienced during crystallization of the nodule. (a) The olivine grain appears to be growing towards the plagioclase-plagioclase junction with little or no associated growth of the plagioclase. If this were to continue to completion, the olivine would inherit the impingement angle. (b) Note how the olivine-plagioclase grain boundaries curve towards the planar-sided pockets of melt (now glass), indicating simultaneous growth of both phases. (c) A cartoon showing the progressive growth of a second phase into a pore bounded by two plagioclase grains that are not growing: This results in the second phase inheriting the geometry of the pore (i.e., the situation illustrated in Figure 11a). (d) If the plagioclase walls grow at the same time as the second phase grows into the pore, the resultant angle at which the grain boundaries meet is higher than that at which the two original plagioclase grains intersect (i.e., the geometry becomes that illustrated in Figure 11b).

conditions required for augite growth into progressively narrower pores: we suggest the radius of curvature effect matters more at the much higher under-coolings we see in the margin, and is less important in the sill centers where the lower under-coolings mean that the relative rates of plagioclase and augite growth are the predominant controls. The details of the balance of these different processes on the final dihedral angle deserve further study and this will be the subject of a later contribution.

4.4.3. Timing of Dihedral Angle Formation

[53] The recognition that the geometry of three-grain junctions is determined by factors operating during solidification provides the potential to use Θ_{cpp} as a quantitative measure of cooling rate during the interval over which the cpx-plag-plag junctions are being formed. Evidence from the lava lakes shows that angles start being formed in appreciable numbers in basaltic systems at >1120°C, and that they are all formed by the time the temperature has dropped to 940–920°C. Importantly, the solidified crust of the lava lake (i.e., that part in which Θ_{cpp} has attained the final value of 78°) contains ~10 vol.% non-crystalline material, predominantly filling narrow pores. This suggests that the population of cpx-plag-plag dihedral angles, at least in rapidly cooled mafic bodies, has reached its final form while there is still some liquid present. That this may also be the case for more slowly cooled dolerites is suggested by the presence of granophyric pockets in coarse-grained dolerites (e.g., Figure 7e) – these

are the slowly cooled equivalents of the glassy pockets of silica-rich liquid in the lava lake crust and crystallized at <700°C [e.g., *Larsen and Tegner*, 2006]. We consider it likely that the final value of Θ_{cpp} (corresponding to complete solidification at plagioclase-plagioclase-pyroxene junctions) in these slowly cooled dolerites will have been reached well above 700°C.

[54] The silica-rich pockets of glass/granophyre in the (non-fractionated) dolerites are absent in adcumulates in fractionated layered intrusions. Adcumulates have suffered (almost) complete loss of rejected solute; the formation of dihedral angles in slowly cooled fractionating systems may therefore not be directly comparable to that in non-fractionated dolerites. An adcumulate comprising only plagioclase and pyroxene will only attain its final population of dihedral angles when the rock is entirely solid, while the final population of angles in an orthocumulate will be attained while some liquid still remains. The implications for mass transport during solidification and its effects on the dihedral angle population will be discussed further in a later contribution.

4.5. Summary: The Igneous Process

[55] In contrast to previously published work, our new observations demonstrate that the geometry of three-grain junctions in dolerites and gabbros is primarily formed during solidification and is controlled by the relative rates of growth of the minerals at the junction. This in turn is affected by the
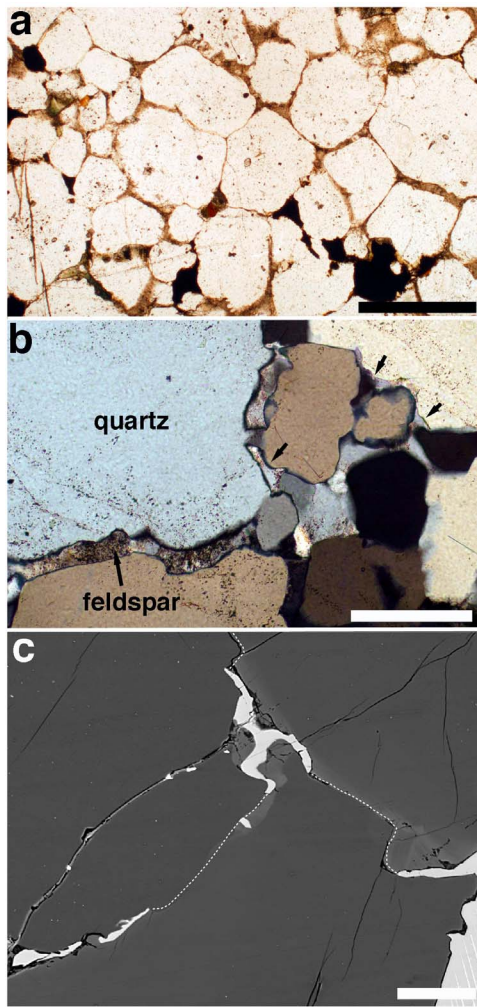
Figure 12. Quartzo-feldspathic migmatites containing originally melt-filled pores that have been filled by feldspar. (a) Contact-metamorphosed banded iron formation from the aureole of the Duluth Complex, Minnesota, with rounded restitic quartz grains (colorless) separated by cuspate, highly turbid network of feldspar. The topology of the feldspar is highly reminiscent of the melt topology in texturally equilibrated systems, suggestive of melt-solid equilibrium before crystallization of the melt-filled porosity. The scale bar is 1 mm long. (b) Contact metamorphosed Archean gneiss from the aureole of the Rum Layered Igneous Complex. Scale bar is 200 μm long. Note the cuspate shape of the feldspar (particularly cuspate grains are arrowed), and the rounded restitic quartz. (c) Backscatter electron image of gabbro from the Middle Zone of the Skaergaard Layered Series, showing cuspate augite grains (pale gray) on plagioclase (mid-gray) grain boundaries (marked by white dotted lines). These cuspate grains are known as fish-hook augites [*Morse and Nolan*, 1984] and are always associated with anomalously anorthitic plagioclase (note the paler gray plagioclase on one side of each grain boundary). The scale bar is 50 μm long.

rate of cooling, both because growth mechanisms and growth rates of each phase involved are dependent on the extent of under-cooling, and because the necessary mass transport in the liquid phase is controlled by absolute temperature as well

as the connectivity of the liquid. The population of cpx-plag-plag dihedral angles in rapidly cooled dolerites is not the same as the plagioclase-melt dihedral angle population because the narrower pores are unlikely to fill with pyroxene: Θ_{cpp} is ~78° in these rocks. Dolerites that solidified over longer time-scales have higher Θ_{cpp}, because of changes in the relative rates of growth of clinopyroxene and plagioclase during the last stages of formation of three-grain junctions. The final population of cpx-plag-plag junctions in dolerites is completely formed when the rock is ~90% solidified. In contrast the final population in adcumulates is not likely to be completely formed until the rock is ~100% solidified. The extent to which these primary dihedral angle populations are modified subsequent to solidification is discussed in the remainder of the contribution.

5. Secondary Formation of Dihedral Angles: The Metasomatic Process

[56] Cpx-plag-plag junctions in dolerites and lava lakes are almost invariably formed by either planar plagioclase-pyroxene boundaries, or by boundaries that are convex (with respect to the pyroxene) in the immediate vicinity of the junction (Figure 11). Concave curvature (i.e., cuspate pyroxene grains, leading to smaller angles) is extremely rare. There is, however, one geological environment in which concave curvature is the norm rather than the exception.

[57] Cuspate grains at the junctions of three larger grains are common in high-grade metamorphic rocks [*Sawyer*, 1999; *Marchildon and Brown*, 2002; *Holness and Sawyer*, 2008] and are used as a diagnostic indicator of partial melting (Figures 12a and 12b). The current interpretation of these cuspate grains is that they solidified from a silicate melt, filling in a pore geometry that was in melt-present textural equilibrium. Their cuspate shape and low dihedral angles are inherited. *Holness and Sawyer* [2008] showed that the cuspate morphology is partly a consequence of nucleation inhibition in small pores, with a delay in the full crystallization of the melt leading to textural equilibration of the pore walls.

[58] These microstructures are not generally seen in mafic intrusive rocks. This may be because their development requires much slower cooling rates (and a lower undercooling) than are commonly experienced by mafic intrusions in the shallow crust. While similar microstructures may be present in more slowly cooled gabbro bodies emplaced in the deep crust, exhumation is likely to involve orogeny with associated regional metamorphism and a consequent overprinting of early microstructure. However, cuspate augite grains are locally present in several layered intrusions.

5.1. The Rum Eastern Layered Intrusion

[59] The Rum Igneous Complex is part of the North Atlantic Tertiary Igneous Province, and comprises a group of related layered intrusions that are thought to have underlain a large central volcano [*Emeleus et al.*, 1996]. The Eastern Layered Intrusion comprises 16 macro-units each formed of an underlying olivine cumulate (peridotite) and a series of overlying troctolitic and gabbroic cumulates (known by the local name of allivalite) (Figure 13a). The bases of several of the plagioclase-bearing cumulate horizons are marked by localized metasomatism by upwardly migrating liquids

sourced from the underlying peridotite. Evidence for the metasomatism includes 10 cm irregular finger structures [*Butcher et al.*, 1985; *Morse et al.*, 1987], macro-scale modal discontinuities caused by mobilization of clinopyroxene over distances of up to 10 m [*Holness et al.*, 2007d; *Sides*, 2008], changes to primocryst compositions [*Tait*, 1984, 1985; *Holness*, 2007], and anomalously low values of Θ_{cpp} associated with distinctive cuspate augite grains [*Holness*, 2007].
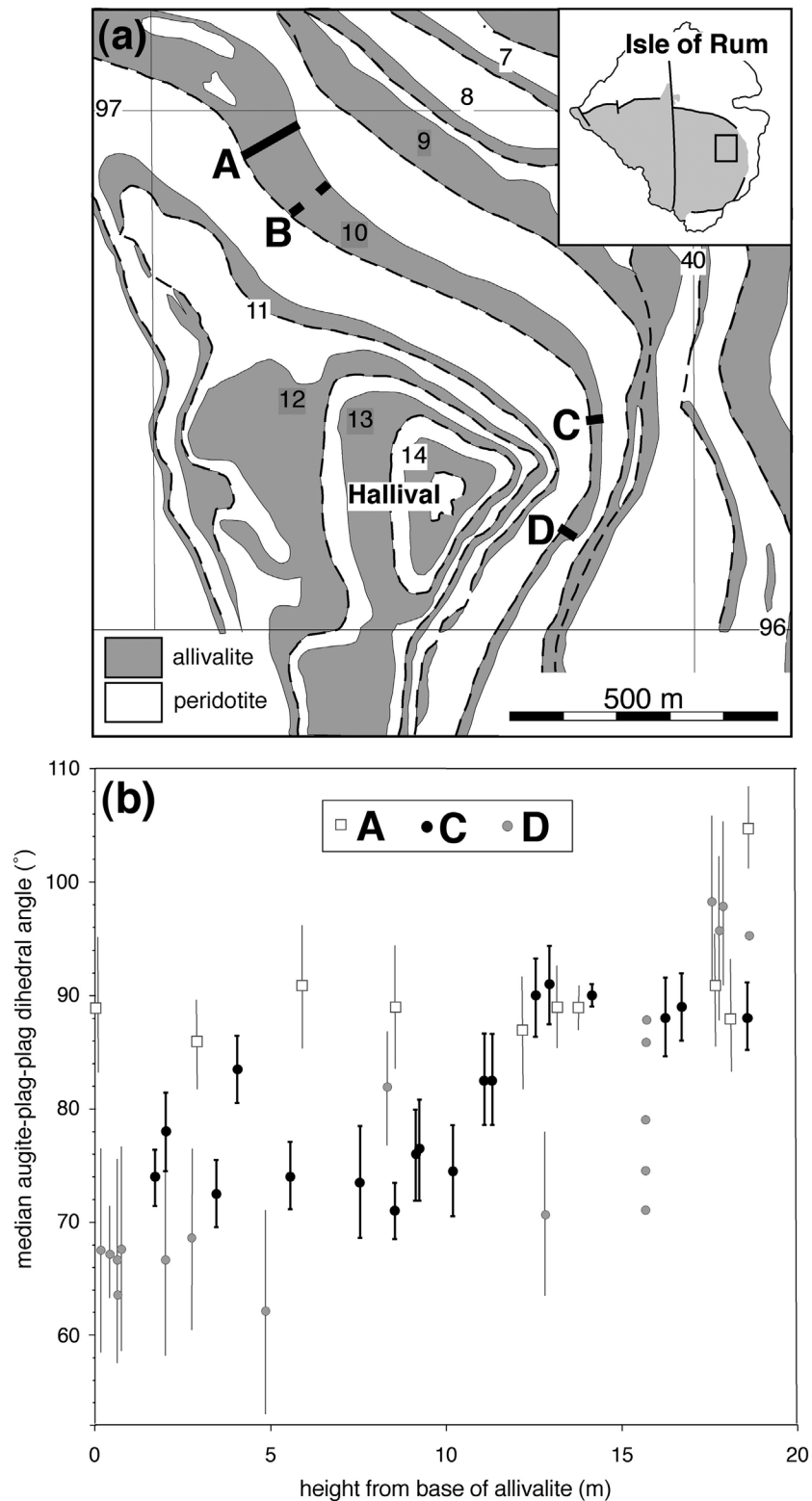

Figure 13

Table 5. Modal Composition and Dihedral Angle Data for the Unit 10 Allivalites of the Rum Eastern Layered Intrusion at Grid Reference NM3985 9642

Sample	Height[a]	Plagioclase[b]	Olivine	Augite	n[c]	Θ_{cpp}[d]	Standard Deviation	Skew	Augite Habit
N4	1.7	66.0	13.2	20.7	199	74 ± 2.5	21.1	−0.5	poikilitic
N9	2.15	52.2	13.6	34.1	181	78 ± 2.5	17.1	−0.6	cumulus
N32	3.44	63.5	18.9	17.6	100	72.5 ± 3	20.5	−0.6	poikilitic
N34	4.04	67	10.7	22.3	100	83.5 ± 3	18.7	−0.9	cumulus
N35	5.54	68.6	9.0	22.3	100	74 ± 3	18.3	−1.2	cumulus
N38	7.52	50.2	10.3	39.5	100	73.5 ± 5	19.3	−0.2	cumulus
N39	8.52	55.5	9.8	34.7	100	71 ± 2.5	22.1	−0.4	cumulus
N40	9.12	52.1	9.0	38.9	100	76 ± 4	17.9	−0.1	cumulus
N41	9.22	51.7	6.9	41.4	100	76.5 ± 4.5	19.1	−0.5	cumulus
N42	10.17	57.8	13.7	28.5	100	74.5 ± 4	22.9	−0.4	cumulus
N18	11.05	-	-	-	100	82.5 ± 4	19.2	−0.6	cumulus
N45	11.27	54.9	13.4	31.7	100	82.5 ± 4	20.4	−0.9	cumulus
N47	12.52	58.9	3.4	37.7	100	90 ± 3.5	14.1	−0.4	cumulus
N48	12.92	-	-	-	100	91 ± 3.5	15.0	−1.5	cumulus
N49	14.12	58.4	13.2	28.4	200	90 ± 1.5	12.9	−1.0	cumulus
N52	16.22	43.2	54.0	2.0	100	88 ± 3.5	17.3	−1.3	Interstitial only
N53	16.67	61.1	37.1	1.8	100	89 ± 3	17.0	−1.3	Interstitial only
N55	18.57	51.6	31.2	17.2	100	87 ± 3	17.-	−0.1	cumulus

[a]The stratigraphic distance from the underlying Unit 10 peridotite in meters.
[b]All modes are given in vol.%.
[c]The number of measurements for each sample
[d]The error on the median is the 95% confidence interval calculated according to the method of *Stickels and Hücke* [1964].

Holness [2007] further identified a coarse-grained gabbroic facies underlying some of the infiltrated allivalites that she suggested was the solidified remains of ponded late-stage interstitial liquids derived from the underlying peridotite.

[60] The values of Θ_{cpp} are essentially bimodal in the Rum allivalites, with values of about 80° in the troctolites and 90° in the gabbros [*Holness*, 2005; *Holness and Winpenny*, 2009; *Holness et al.*, 2007a], comparable with the step-change in Θ_{cpp} observed at the transition from olivine-plagioclase cumulates to olivine-plagioclase-augite cumulates in the Skaergaard Layered Series [*Holness et al.*, 2007a]. The base of the allivalites of Units 8, 9 and 10 have lower Θ_{cpp} than that expected for their cumulus assemblage [*Holness*, 2005; *Holness et al.*, 2007d; *Holness*, 2007; *Sides*, 2008].

[61] Unit 10 has been used as the type unit for the Rum Eastern Layered Intrusion [*Brown*, 1956] (sampled along traverse *A* in Figure 13a). However, the crystallization history of Unit 10 was far from straightforward: *Tait* [1984, 1985] found geochemical evidence for infiltration at traverse *D* (Figure 13a), associated with abundant cuspate augite grains and Θ_{cpp} of 65–72 [*Holness*, 2007] (Figure 13b).

[62] A new traverse was made across the Unit 10 allivalite, from grid reference (NM39830 96422) to (NM39809 96424) (traverse *C* in Figure 13a). Samples were collected at approximately 1 m intervals through the 18.6 m thickness of this unit. The uppermost 5 m of the Unit 10 peridotite are exposed at this locality. Gabbroic pegmatite is present below the base of the allivalite 8 m north of the traverse, similar to that described by *Holness* [2007]. Mineral modes were determined by point counting 1000–2200 points per sample (Table 5). Allivalite is dominated by cumulus plagioclase (>50 vol.%) with a preferred orientation parallel to the modal layering. Augitic clinopyroxene generally accounts for 20–40 vol.%, with two (troctolitic) exceptions. Augite is generally granular (Figures 14a and 14b) apart from the lowermost 1.35 m in which it is poikilitic. Augite also forms rinds around cumulus olivine grains and as small interstitial grains at plagioclase triple junctions. The samples in the lower half of the allivalite are noticeable for the well-developed elongate and cuspate apophyses extending from cumulus augite grains down plagioclase-plagioclase grain boundaries, similar to those found in Traverse *D* by *Holness* [2007] (Figure 14c). Interstitial augite is commonly cuspate (Figure 14d). Very rarely, cuspate polycrystals occur at plagioclase triple junctions (Figure 15). These features are not present in Brown's type traverse (*A*).

[63] In the lower ∼10 m of the allivalite Θ_{cpp} is generally <80°, whereas in the upper parts Θ_{cpp} falls between 87° and 91° (Table 5). There are two transitional samples about 11 m from the underlying peridotite with Θ_{cpp} of 82.5° (Figure 13b). The spatial variation of Θ_{cpp} is different in

Figure 13. (a) A simplified geological map of part of the Eastern Layered Intrusion [from *Emeleus*, 1994], showing the macro-scale interlayering of allivalite (troctolitic and gabbroic cumulates) and peridotite (olivine cumulates). The four traverses across the Unit 10 allivalite are: A – collected and described by *Brown* [1956]; B – collected and described by *Holness et al.* [2007b]; C – collected as part of the present study; D – collected and described by *Tait* [1984, 1985]. The grid lines and numbers refer to the National Grid and are spaced 1 km apart. (b) The variation of Θ_{cpp} as a function of stratigraphic height in the Unit 10 allivalite. Data from Table 5, together with previously published data from traverses A [*Holness et al.*, 2007b] and D [*Holness*, 2007], normalized to a thickness of 18.6 m to match that of traverse C. The five data points for traverse D plotted at ∼15 m height were collected from a layer-parallel traverse [*Tait*, 1984]. The error bars give the 95% confidence interval, and are newly calculated for the previously published data.
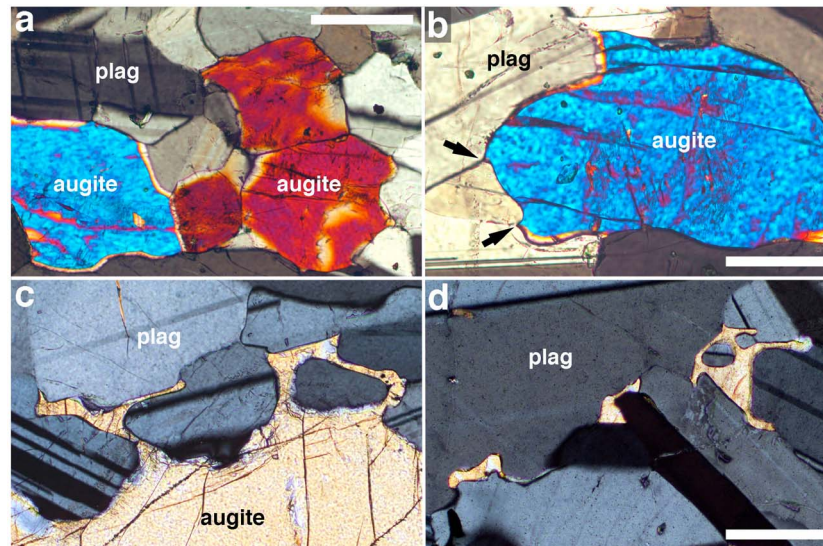
Figure 14. Photomicrographs of gabbroic cumulates from the Unit 10 allivalite, Rum Eastern Layered Intrusion. The scale bar in each image is 200 μm long. (a) Sample N48, collected 12.92 m above the base of the allivalite. Note the compact form of the cumulus augite. (b) Sample N47, collected 12.52 m above the base of the allivalite. Note the well-defined dihedral angles (arrowed) with slight asymmetry. Θ_{cpp} in this sample is 90 ± 3.5°. (c and d) Sample N32, collected 3.44 m above the base of the allivalite. The cumulus grain occupying the lower part of the image in Figure 14c has elongate apophyses extending down adjacent plagioclase-plagioclase grain boundaries, with low dihedral angles. Figure 14d shows samples from the lower 11 m of the allivalite contain abundant cuspate interstitial grains, many of which form clusters in optical continuity.

each of the three traverses *A*, *C* and *D* (Figure 13b). Θ_{cpp} in the northernmost traverse (*A*) [*Brown*, 1956] is constant at ~90° except for a few data points within the topmost meter, while that in Tait's traverse (the southernmost) is of the order 70° until the last few meters where it increases to ~100°. The new data, from the traverse between *A* and *D*, fall between these two extremes, with a clear step-change in Θ_{cpp} halfway up the allivalite.

[64] Preliminary analysis of augite composition as a function of height in the Unit 10 allivalite shows that the step-change in Θ_{cpp} is associated with a variation of Ti content [*Sides*, 2008]. The rims of augite cumulus grains above the Θ_{cpp} step have similar Ti concentrations as the grain centers, while those below the step are significantly enriched in Ti compared to the grain centers. The Ti content of the small cuspate augite grains found at plagioclase triple junctions is also significantly higher than that of the centers of cumulus augite grains.

5.2. Discussion

[65] The new results are consistent with those of *Tait* [1984, 1985] and *Holness* [2007], who both suggested that the base of Unit 10 was infiltrated by late-stage fluids derived from the underlying peridotite. Not only is there a nearby patch of coarse gabbro at the base of the allivalite (interpreted by *Holness* [2007] to be a solidified pool of trapped liquid sourced from the peridotite), but the lower parts of the allivalite contain abundant cuspate grains, some of which are polycrystalline, associated with lower than usual Θ_{cpp} for Rum gabbros (~90°) [*Holness*, 2005]. Following *Holness* [2007], the cuspate grains are interpreted as the solidified remains of late-stage melt that infiltrated a previously melt-

free rock, driven along plagioclase three-grain junctions by the consequent reduction in internal energy [*Watson*, 1982; *Stevenson*, 1986; *Hammouda and Laporte*, 2000]. The step change in Θ_{cpp} therefore corresponds to the level to which this fluid penetrated. At traverse *A*, there was no infiltration and the dihedral angles record the primary igneous geometry of three-grain junctions. At traverse *D*, the infiltrating liquid penetrated to the top of the allivalite, completely re-setting the original median dihedral angle by creating a large population of low dihedral angles at cuspate grains. At traverse *C*, the liquid penetrated only halfway, re-setting the primary median value in the lower 11 m of the allivate, while preserving the original angle population in the upper, un-infiltrated, part.
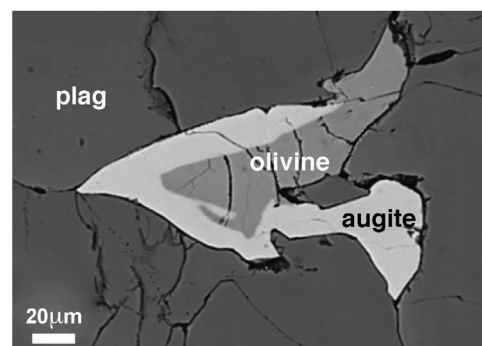
Figure 15. A backscattered electron image of a cuspate polycrystal comprising augite and olivine at the junction between three plagioclase grains in sample N32, from the lower 11 m of the Unit 10 allivalite.

[66] For infiltration to occur it is essential that the solidus of the infiltrating liquid is considerably lower than that of the solidified rock being infiltrated: this is consistent with the generally more evolved composition of the liquid as evidenced by high augite Ti contents. The liquid that formed the pods of coarse gabbro elsewhere under the Unit 10 allivalite apparently got stuck at the permeability barrier created by the allivalite, perhaps because its solidus was too high. The Unit 10 allivalite was thus essentially completely solid but relatively hot, at the time the late-stage cool liquids were expelled from the underlying peridotite.

[67] Other examples of low dihedral angles in mafic rocks are provided by vermicular intergrowths of clinopyroxene and An-rich plagioclase, associated with apatite and reversed rims on plagioclase primocrysts (Figure 12c). These are known as fish-hook augites and were first described by *Morse and Nolan* [1984] form the Kiglapait Intrusion and in more detail by *Holness et al.* [2011] for the Skaergaard Intrusion. These are believed to be the solidified remnants of late-stage liquids, but it is not clear whether these liquids penetrated along previously melt-free grain boundaries or whether they form from the last liquid as those grain boundaries form.

5.3. Summary: The Metasomatic Process

[68] These examples of low dihedral angles are fundamentally different from those in dolerites and lava lakes. The low dihedral angles in the Rum allivalites form during the last stages of microstructural and chemical evolution and involve the migration of relatively low-temperature liquids through an essentially solidified matrix. This is the *metasomatic process.* For a case in which there is time to establish equilibrium melt topology, the driving force for metasomatism is provided by the reduction of interfacial energy. The low angles in the Unit 10 allivalite are consistent with the operation of such a process: the low angles were inherited from a texturally equilibrated melt topology via a pseudomorphing process analogous to that seen in migmatites. This contrasts with the primary dihedral angles formed in doleritic bodies in which the cooling rate is too fast to permit textural equilibration to keep pace with crystal growth: the pore geometry in rapidly cooled examples is controlled entirely by the geometry of growth surfaces and grain impingement.

[69] The similarity between three-grain junctions formed during the metasomatic process and those seen in migmatites is a consequence of both having a small pore size (low volume of liquid) and the low growth rates of the pore walls. In migmatites these low growth rates are due to the slow cooling rates typical of regional metamorphism and to nucleation inhibition in small pores. In the Unit 10 (metasomatic) example, the growth rate is effectively low because the rock the liquid penetrates is already solid. The liquid has a low solidus compared to the host and there is time to approach textural equilibrium. The final solidification history of the infiltrating liquid is directly analogous to the migmatite situation, with overgrowth of the pore walls (i.e., the plagioclase component of the late liquid overgrows the plagioclase forming the walls) and final crystallization of augite (and rare olivine) in the remaining space. The difference is whether the liquid is initially internally or externally sourced.

[70] The features observed in the Unit 10 allivalite are uncommon and we would expect low dihedral angles formed by the metasomatic process to be rare in mafic rocks. It is, however, possible that similar features are present in the mantle, due to the migration of low-temperature liquids [e.g., *Hammouda and Laporte*, 2000], although this might be difficult to test due to later high-temperature recrystallization.

6. Textural Equilibration in the Sub-solidus: The Metamorphic Process

[71] Low dihedral angles formed during solidification are out of equilibrium and are therefore unstable. Given the opportunity, the fully solidified microstructure will evolve toward textural equilibrium. During this process, the microstructural record preserved in mafic rocks will be overprinted to variable extents by sub-solidus modifications: we term this the *metamorphic process.* The metamorphic process is essentially that which modifies the initial (disequilibrium) dihedral angle population in response to textural equilibration in the sub-solidus. For a correct interpretation of rock history it is important to establish the extent to which the primary record of initial solidification or later metasomatism has been modified. Previous work was based on the assumption that *all* mafic rocks with $\Theta_{cpp} > 60°$ (the presumed starting point for dolerites) had undergone sub-solidus modification [e.g., *Holness et al.*, 2005a] but this study demonstrates that this is not the case. Instead, the observations of a significant variation of Θ_{cpp} due to primary processes bring into question whether sub-solidus modification of grain junctions has even occurred at all. Under what conditions are dihedral angles modified by the metamorphic process?

[72] As evident from the first section of this contribution, texturally equilibrated microstructures are seen in a variety of settings, from fine-grained chilled margins of large intrusions, to hornfelses and granulites. But these represent an end-point of microstructural evolution: how did the microstructures get to be this way? *Higgins* [2011] and *Holness and Siklos* [2000] suggest that the approach to textural equilibrium, at least in static situations, begins with the rotation of grain boundaries at triple junctions to form the equilibrium dihedral angle. As the correct dihedral angle is established, the correct interfacial curvature propagates away from the junctions. The final step is the onset of normal grain growth. This is driven by differences in chemical potential of surfaces with different radii of curvature, and by the formation of low-energy, crystallographically controlled grain-boundary segments [*Kruhl*, 2001], and occurs *after* the establishment of the equilibrium dihedral angle population.

[73] This sequence of events is consistent with the experimental work of *Holness et al.* [1991], who described the microstructural evolution in forsterite-calcite aggregates. The forsterite-calcite-calcite dihedral angle changed from the initial value of 120° (formed during the fabrication of the polycrystal by hydrostatic compression) to the equilibrium value of 165° during heating at constant pressure. They were able to track the progressive increase in angle via a series of experiments and demonstrate a clear temperature control on the rate at which it occurred.
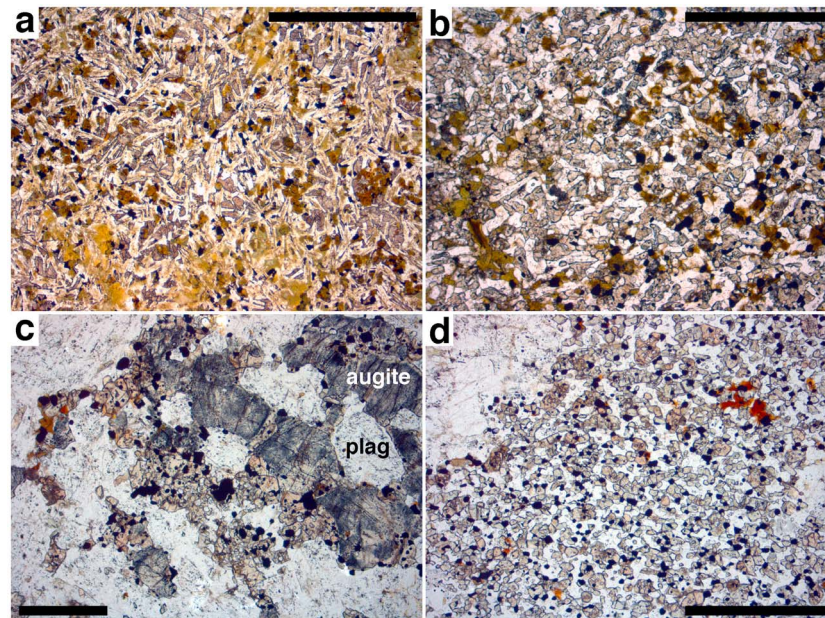
Figure 16. Photomicrographs of mafic rocks from the aureole of the Skye Tertiary Igneous Centre, collected by Fran Entwhistle (University of Leeds). Scale bars in all images are 1 mm long. (a) Basalt with almost complete retention of the original igneous microstructure, comprising randomly oriented plagioclase laths with ophitic augite. Olivine is complete replaced by hydrous phases. (b) Basaltic hornfels. Note the retention of the elongate, randomly oriented plagioclase grains, while the ophitic pyroxene (and olivine) is completely replaced by a granular aggregate of Ca-poor and Ca-rich pyroxene, together with scattered granular oxides. (c) Coarse-grained (gabbroic) enclave in a basaltic lava flow is partially hornfelsed, while the fine-grained matrix (d) is completely recrystallized to a two-pyroxene hornfels. The original coarse plagioclase grains in Figure 16c are unaffected while the original augite crystals are partially replaced by a fine-grained granular aggregate of oxide, two pyroxenes and plagioclase.

[74] Recrystallization of highly deformed rocks, either after or during deformation, can also result in granular equilibrated microstructures. In this case, grain boundary migration is driven by the reduction of internal energy consequent to the creation of defect-free crystals, and it occurs by strain-induced migration of grain boundaries, subgrain rotation, and grain-boundary migration recrystallization (see the comprehensive review by *Vernon* [2004]). However, it is not clear whether the equilibrium dihedral angle is attained by movement of the grain boundaries only in the immediate vicinity of the triple junction, or whether this process is accelerated by wholesale grain boundary migration during either normal grain growth or dynamic/static recrystallization.

[75] Textural equilibrium is commonest in mono-mineralic rocks, or mono-mineralic regions of poly mineralic rocks. This is because equilibration only requires movement of material across grain boundaries, rather than along them. For this reason, textural equilibrium is usually best developed in very fine-grained rocks: these are therefore the obvious place to look for evidence of the metamorphic process. The best natural laboratories for constraining the extent of the metamorphic process are those with variable sub-solidus thermal histories permitting both the preservation of the original microstructure (or in which the original microstructure can be inferred) and a variable degree of modification. Contact aureoles and intraplutonic quench zones are ideal.

6.1. Contact Metamorphism of Mafic Rocks

[76] Basaltic hornfelses are generally in textural equilibrium (e.g., sample V5, Table 1; Figures 2c and 2d) but this microstructure is at least partly generated by reaction and recrystallization rather than grain boundary migration in the basalt. Basaltic hornfels in the aureole of the Skye gabbros (see *Almond* [1964] and *Ferry et al.* [1987] for details) commonly retains the (approximate) original shape of the grains of basaltic plagioclase although the original pyroxene and olivine have been replaced by new pyroxene (±biotite, oxides) (Figure 16). The replacement is a strong function of grain size, with coarser-grained regions retaining the original igneous mineral assemblage while nearby fine-grained regions are completely replaced (Figures 16c and 16d). At any given grain size plagioclase generally survives for longer than the mafic phases. The close approach to textural equilibrium is most probably a reflection both of the high temperatures of contact metamorphism and of the multivariance of the reactions in metabasites (which means the mineral assemblages remain the same over a wide range of temperature) [*Tracy and Frost*, 1991]: the microstructure can therefore undergo appreciable grain growth and equilibration.

6.2. Intra-plutonic Quench Zones

[77] Fine-grained basaltic rocks that have undergone heating *without* reaction can be found in the chill zones of
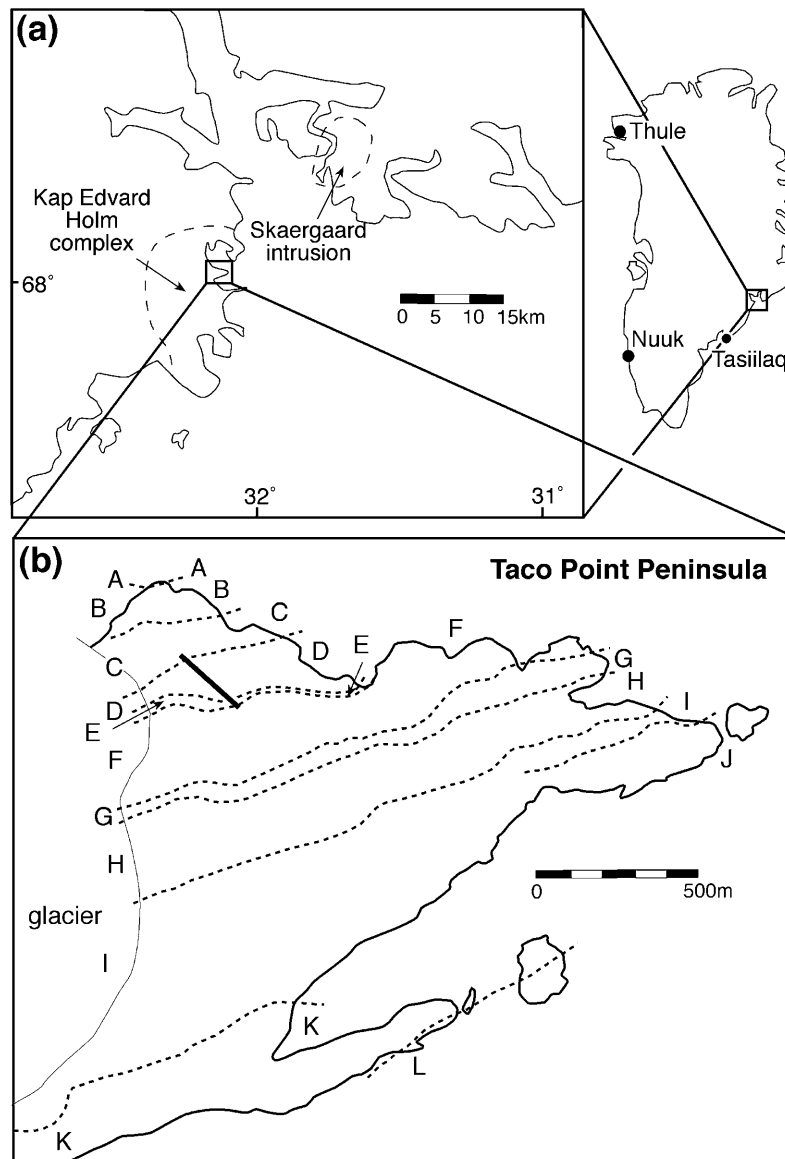
Figure 17. (a) Map showing the relative positions of the Skaergaard and Kap Edvard Holm intrusions on the east coast of Greenland (with location shown on the inset map). (b) The Taco Point area of the Kap Edvard Holm intrusion is enlarged, which shows the macrorhythmic units described by *Tegner et al.* [1993]. The heavy line shows the location of the sample traverse.

large intrusions. Sample 114425 (a fine-grained igneous rock from the margin of the Bushveld Intrusion; Table 1; Figures 2e and 2f) contains the elongate, randomly oriented plagioclase grains expected for rapidly crystallized basalt, but the pyroxene grains are rounded with equilibrated triple junctions. Importantly the mineral mode is igneous, so the original microstructure (which is likely to have been comparable to that of the Traigh Bhàn na Sgùrra sill) must have been modified in the sub-solidus in the absence of reaction and recrystallization. The extensive microstructural modification is most likely a consequence of the fine grain-size of the chill zone and because it was held at relatively high temperatures for a sufficiently long time. A further factor may have been a low original Θ_{cpp} (likely to be ~78°): the driving force for equilibration is higher the further the initial

state is from equilibrium so rocks with the lowest angles are more susceptible to modification than those with higher initial Θ_{cpp}. The change from a microstructure typical of a rapidly cooled dolerite (e.g., Figures 7a and 16a) to that observed in Figures 2e and 2f was effected by the metamorphic process. A more complete picture of this transformation can be obtained from a suite of related rocks from an intraplutonic chill zone.

[78] The (>300 km^2) Kap Edvard Holm Layered Gabbro Complex is on the opposite side of Kangerdlugssuaq Fjord from the Skaergaard Intrusion (Figure 17a). Variations of mineralogical composition are restricted in the intrusion, despite a cumulate thickness of at least 5 km [*Deer and Abbott*, 1965], due to repeated replenishment of the open-system magma chamber [*Bernstein et al.*, 1992]. A 1000 m thick
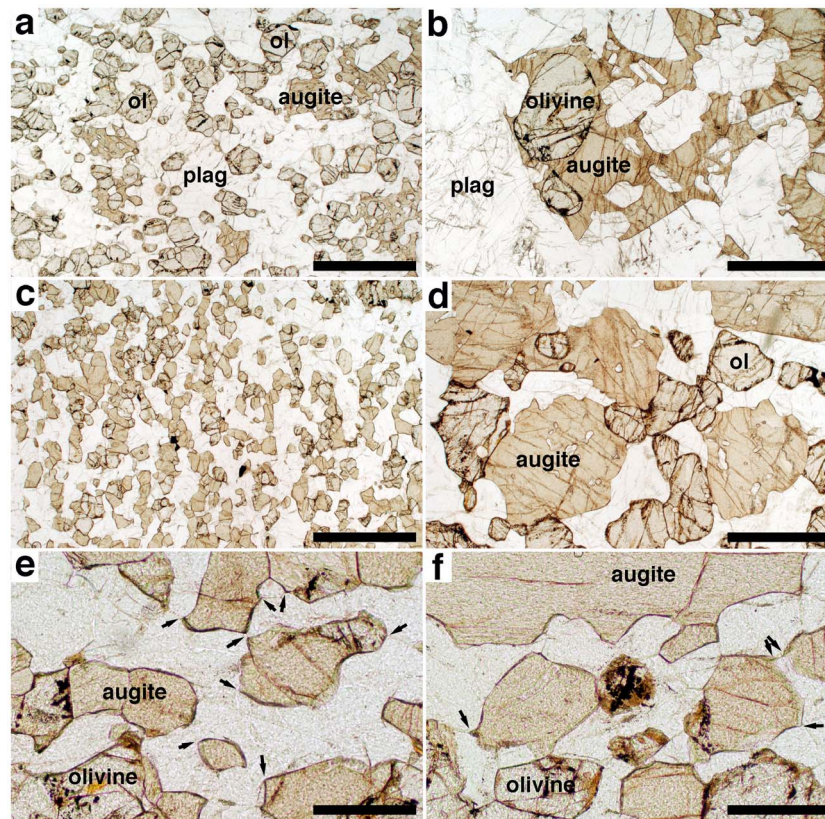
Figure 18. Photomicrographs of the Kap Edvard Holm gabbros. (a) Sample 30, base of macro-rhythmic unit D, $\Theta_{cpp} = 103 \pm 2.5°$. Note the granular olivine and the compact oikocrysts of augite. Scale bar is 1 mm long. (b) Sample 33b, upper part of macro-rhythmic unit D, $\Theta_{cpp} = 92 \pm 1.5°$. Augite is poikilitic in this unit, with included plagioclase and olivine grains. Scale bar is 1 mm long. (c) Sample 41, base of macro-rhythmic unit E, $\Theta_{cpp} = 101 \pm 1.5°$. All three phases are granular in this chill zone. Scale bar is 1 mm long. (d) Sample 46, upper part of macro-rhythmic unit E, $\Theta_{cpp} = 92 \pm 2°$. Augite is compact and granular but has significant numbers of included plagioclase grains. Scale bar is 1 mm long. (e) Sample 41. Cpx-plag-plag dihedral angles are generally high (arrowed). Scale bar is 200 μm long. (f) Sample 46. This contains a significant number of low cpx-plag-plag dihedral angles (examples are arrowed). Scale bar is 200 μm long.

section of gabbros exposed on Taco Point [*Tegner et al.*, 1993] comprises 12 macrorhythmic units, varying in thickness from $\sim$8 m to 150–200 m, with an average of $\sim$80 m (Figure 17b). Each macrorhythmic unit has a very sharp basal contact between an underlying medium-grained (>1 mm) modally layered olivine gabbro and an overlying fine-grained (<0.5 mm) aphyric, massive or weakly layered, basaltic rock. The fine-grained basaltic layers are 0.5–3 m thick, grading into olivine gabbro which commonly has well-developed, small-scale modal layering. These contacts have been interpreted as intraplutonic quench zones formed by the rapid crystallization of a separate injection of magma into the Kap Edvard Holm chamber [*Tegner et al.*, 1993; *Tegner and Wilson*, 1995]. Individual quench zones are thought to be the products of rapidly cooled, hot, dense, inflowing magma as it propagated along the chamber floor, displacing the resident magma upwards in a manner suggested by *Huppert and Sparks* [1981] [*Tegner et al.*, 1993].

[79] We examined a suite of 16 samples collected perpendicular to layering across three of the rhythmic units on Taco Point, covering nearly 60 m of stratigraphy and crossing units *D* and *E* in their entirety with a single sample

from the base of unit *F* (Figure 17b). Geochemical and petrographic data can be found in *Tegner et al.* [1993] and *Tegner and Wilson* [1995]. The samples all contain cumulus plagioclase and olivine. In rhythmic unit *D*, augite forms oikocrysts enclosing plagioclase and olivine (Figures 18a and 18b), while in Unit *E* augite is granular (Figures 18c and 18d). Augite grains are transitional in Unit *F*, with compact cores and abundant enclosed plagioclase grains in the margins. The grain size is a strong function of stratigraphic height, with fine-grained rocks at the base of each unit (Figures 18a, 18c, and 18e) coarsening upwards. The plagioclase grains enclosed by augite oikocrysts are rounded at the base of Unit *D*, but have well-defined planar growth surfaces in the coarser-grained upper parts of Unit *D*. We measured up to 100 individual augite-plagioclase-plagioclase dihedral angles in each of the 16 samples. The details of the populations are given in Table 6, together with the average grain size of the cumulus olivine grains.

[80] The dihedral angle varies with stratigraphic position, with high Θ_{cpp} near the base of each macro-rhythmic unit, decreasing with stratigraphic height toward values typical of gabbroic cumulates in the Rum Eastern Layered Intrusion

Table 6. Details of the Sample Set Through the Kap Edvard Holm Macro-rhythmic Units at Taco Point

Sample	Stratigraphic Height	Macro-rhythmic Unit	n^a	$\Theta_{cpp}{}^b$	Standard Deviation	Skew	Average Grain Size^c (mm)
30	1.0	D	100	103 ± 2.5	8.6	0.3	0.15
34	1.4	D	100	101 ± 2	10.0	−0.5	0.20
36	12.0	D	100	96 ± 1.5	10.3	0.8	1.20
37	27.0	D	100	94 ± 2	10.4	0.1	1.10
32	36.5	D	56	92 ± 2.5	11.8	−1.3	1.25
33	37.5	D	100	92 ± 1.5	11.3	0.3	1.30
38	41.0	D	100	92 ± 1.5	9.4	0.2	1.15
39	46.0	D	80	91 ± 2	10.2	0.3	1.05
40b	48.1	E	100	102 ± 2	9.4	−0.4	0.25
41	48.5	E	100	101 ± 1.5	6.7	0.4	0.23
42	49.2	E	100	100 ± 2	9.8	−1.2	0.25
43	50.4	E	100	99 ± 2	9.0	−0.4	0.25
44	51.0	E	100	97 ± 2	9.0	0.5	0.35
45	52.4	E	100	95 ± 1.5	10.6	−0.9	0.55
46	54.1	E	70	92 ± 2	9.2	−0.5	0.60
47	55.0	F	100	100 ± 2.5	11.1	0.1	0.40

[a]The number of dihedral angle measurements per sample.

[b]The errors on Θ_{cpp} are the 95% confidence interval, calculated according to *Stickels and Hücke* [1964].

[c]From *Tegner et al.* [1993].

(Figure 19a). This pattern is strongly correlated with grain size, with higher Θ_{cpp} in the finer-grained rocks (Figure 19b).

[81] The high Θ_{cpp} is associated with a granular microstructure, close to that expected for textural equilibrium, but very different to that expected for rapid quench crystallization (Figures 18a and 18c). The fine-grained chill zones of the Kap Edvard Holm macro-rhythmic units are therefore closer to solid-state textural equilibrium than their coarser-grained equivalents some meters higher in the stratigraphy. The microstructures in each macro-rhythmic unit are otherwise similar, with the augite habit the same in both the chilled rocks and their coarse-grained equivalents (poikilitic in Unit D, granular in Unit E and transitional in Unit F). This suggests that the higher Θ_{cpp} is not a result of wholesale recrystallization, but is due to localized, sub-solidus, adjustment of grain boundaries in the vicinity of triple junctions via the metamorphic process. We suggest that the smooth decrease in Θ_{cpp} with stratigraphic height within each unit is a complex function of (a) the increasing grain size which increases the diffusion distance necessary for microstructural change, (b) a reduction in the length of time over which the metamorphic process could act: the earliest-solidifying horizons had more time to evolve compared to the overlying horizons, and (c) the greater departure from equilibrium of the dihedral angles in the rapidly crystallized chilled base. This analysis of the Kap Edvard Holm macro-rhythmic units suggests that the metamorphic process plays only a limited role in controlling Θ_{cpp} in (coarse-grained) gabbros, essentially requiring a fine grain size to be effective over the timescales relevant to mafic intrusions in the shallow crust.

6.3. Sub-solidus Microstructural Modification of Gabbro

[82] How important is the metamorphic process for coarse-grained gabbros in layered intrusions? An indication is provided by intrusions containing a clearly identifiable, localized heat source, such as the Rum Eastern Layered Intrusion. *Holness* [2005, 2007] and *Holness and Winpenny* [2009] have shown that Θ_{cpp} in the uppermost parts of each allivalite horizon is elevated compared to the underlying allivalite. This is attributed to the heating effects of the hot, picritic liquid that entered the chamber and formed the overlying peridotite cumulates. As the hotter magma replaced the relatively cool basaltic liquid on the chamber floor it provided the extra heat necessary to promote textural equilibration in the underlying allivalitic cumulates. The length-scales over which the allivalite is affected by the heat of the replenishing picrite are variable, with most horizons affected only within a few centimeters of the overlying peridotite (e.g., unit 12 [*Holness and Winpenny*, 2009]). A similarly short lengthscale is observed under the quench zones of Kap Edvard Holm, with no effect on the uppermost sample of each rhythmic unit (collected some meters from the overlying quench zone). A notable exception is observed in the allivalite underlying the Unit 9 peridotite. This peridotite body is unusual in that it crystallized from a 20 m thick picritic sill emplaced into the mush zone [*Bédard et al.*, 1988; *Holness*, 2005; *Holness et al.*, 2007d]. The allivalite underlying this small intraplutonic intrusion has elevated Θ_{cpp} within 3 m of the contact [*Holness*, 2005; *Holness et al.*, 2007d], while the overlying allivalite has been significantly metasomatised, *Holness et al.* [2007d]. Importantly the grain size in the allivalite is coarse throughout.

[83] Our new understanding of the role of primary solidification on dihedral angles brings more insight to these variable effects. We speculate that the limited modification of Θ_{cpp} below the majority of the peridotite horizons on Rum was a consequence of the metamorphic process acting on an essentially solidified chamber floor consequent to the arrival of hot picritic magma in the chamber. In contrast, the much more marked modification of Θ_{cpp} beneath the Unit 9 peridotite may have been a consequence of a reduced crystallization rate in the underlying gabbroic mush zone, leading to higher dihedral angles formed by the igneous process.

[84] A further example that may record the metamorphic process is provided by oikocrysts. *Holness et al.* [2005a] demonstrated that the clinopyroxene-olivine-olivine dihedral angles in the centers of augite oikocrysts in peridotite cumulates of the Rum Eastern Layered Intrusion are significantly higher than those on their margins. Similar results are
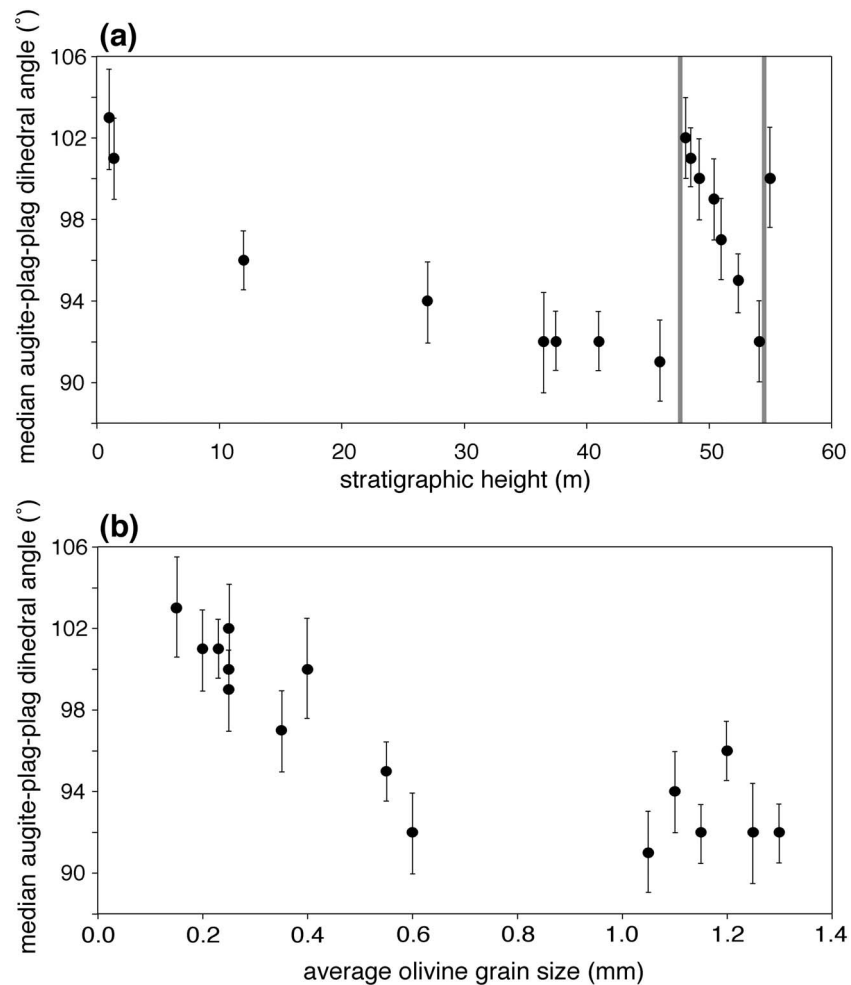
Figure 19. (a) Θ_{cpp} as a function of stratigraphic height through a series of three intraplutonic quench zones from the Kap Edvard Holm intrusion. The zero point on the stratigraphic height marks the base of the lowermost quench zone (rhythmic unit D), while the two gray vertical lines mark the bases of the overlying two quench zones (rhythmic units E and F). (b) The average grain size of cumulus olivine grains as a function of Θ_{cpp}.

found for Θ_{cpp} in augite oikocrysts enclosing plagioclase grains. Figure 20 shows the frequency distributions of augite-plagioclase-plagioclase dihedral angles in a poikilitic gabbro collected from the Unit 9 allivalite of the Rum Eastern Layered Intrusion: Θ_{cpp} inside the oikocrysts is 106 $\pm$ 6°, while that outside is 94 $\pm$ 2.5°. Comparison with the results for the Portal Peak sill suggests that, if this variation were a consequence of the igneous process, the crystallization rate of the oikocryst in the early stages of its growth (i.e., in its central region) would need to be higher than that of the later parts. This could be accounted for by an increase in the extent of under-cooling during progressive solidification [e.g., *Kirkpatrick*, 1981]. However, two lines of evidence point to the metamorphic process being responsible for the intracrystalline variation of dihedral angles. First, the enclosed plagioclase grains are rounded compared to those outside the oikocrysts (Figure 21a): this is most likely due to grain boundary migration driven by the minimization of interfacial area (i.e., sub-solidus textural equilibration [*Vernon*, 1970; *Holness et al.*, 2005a]). The microstructure

inside the oikocrysts therefore has been affected by significant sub-solidus modification: dihedral angles have undoubtedly been changed during the process of rounding the grain shape. Second, the inflected curvature of olivine-augite and plagioclase-augite grain boundaries (Figures 21b– 21d) is indicative of a widening of the dihedral angle associated with the propagation of the new interfacial curvature away from the triple junction [cf. *Holness and Siklos*, 2000]: it is unlikely to be caused by a unimodal variation in the relative rates of olivine and augite growth (c.f. the plagioclase-augite junctions in the Portal Peak sill) because extrapolation toward the three-grain junction of the boundaries far from the junction would imply that the olivine grains were not in contact during earlier stages of the solidification (Figure 21c). Instead it is most likely to have been caused by grain boundary migration in response to subsolidus textural equilibration. This inference is supported by the similarity of these microstructures to those seen in migmatites (Figure 21d).
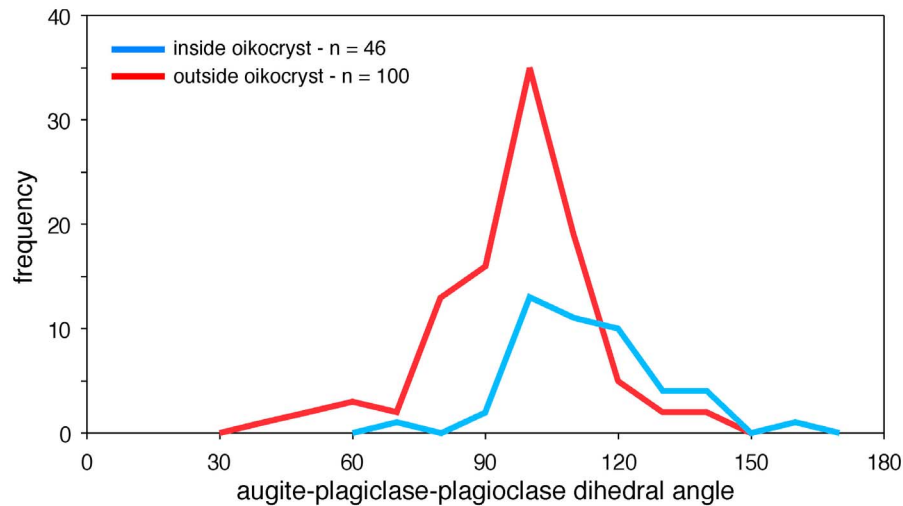
Figure 20. The frequency of dihedral angles in poikilitic gabbro (sample E14) from the Unit 9 allivalite of the Rum Eastern Layered Intrusion. The number of individual measurements is given by *n.* The angles inside augite oikocrysts are generally higher than those outside.

6.4. Summary: The Metamorphic Process

[85] The metamorphic process results in the sub-solidus modification of dihedral angles by the rotation of grain boundaries in the immediate vicinity of the three-grain junction. It is accompanied by progressive modification of grain boundary curvature far from the three-grain junction (Figure 21). It is most effective in fine-grained rocks because the distances required for mass transport are shorter. For any
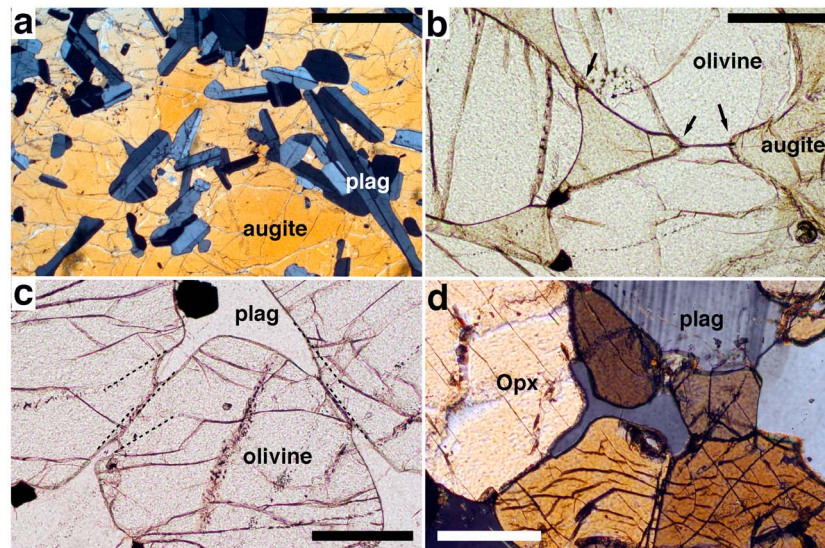
Figure 21. Photomicrographic evidence for the metamorphic processes acting in gabbros. (a) Sample E14, a poikilitic gabbro from the Unit 9 allivalite of the Rum Eastern Layered Intrusion, photographed under crossed polars. The randomly oriented plagioclase grains included by the augite oikocryst are significantly rounded in comparison to the expected growth shape (c.f. Figures 3, 5 and 7). Scale bar is 1 mm long. Figures 21b and 21c depict sample PB2, a peridotite cumulate from the Rum Eastern Layered Intrusion. (b) Note the rounded nature of the interstitial augite grain, with high dihedral angles (arrowed). Scale bar is 200 μm long. (c) Olivine cumulus grains enclosed by plagioclase, with two grains of cumulus Cr-spinel (opaque). The three-grain junctions display significantly different curvature to that expected for impingement, and the extrapolation of the interface (dotted lines) suggests that if these were formed by the igneous process then the olivine grains were not originally in contact. Scale bar is 200 μm long. (d) A highly cuspate plagioclase grain in a granulite from the Nemiscau subprovince, Canada, which is inferred originally to have had low dihedral angles against the surrounding orthopyroxene (Opx) most likely inherited from an original melt-filled pore. However, the plagioclase has developed bulbous ends as the dihedral angle increased toward solid-state textural equilibrium. The scale bar is 200 μm long.

given grain size, the metamorphic process is likely to be most effective if the original dihedral angle population is far from solid-state textural equilibrium. In gabbroic intrusions in the shallow crust its influence is seen most clearly in chill zones. It has limited effect on coarse-grained rocks on the time-scales over which km-scale crustal intrusions cool: the variation of Θ_{cpp} observed in the Rum and Skaergaard gabbros is therefore almost entirely due to the igneous process.

[86] It is pertinent at this point to ask why the metamorphic process can act so effectively during the growth of oikocrysts but has no effect on augite-plagioclase junctions on oikocryst rims and outside the oikocrysts. Oikocryst growth implies limited nucleation, with growth centered on a few scattered sites. Oikocrysts therefore grow before (and at a higher temperature than) interstitial augite elsewhere in the rock. The observed difference in dihedral angle populations is consistent with a very high closure temperature for the metamorphic process in coarse-grained rocks.

7. Conclusions

[87] Disequilibrium microstructures are key to understanding rock evolution as they preserve a record of rock history. We have set out a new framework for understanding disequilibrium dihedral angles in mafic rocks, correcting earlier work which was based on the assumption that all dihedral angle variation is a consequence of sub-solidus modification. This more comprehensive examination of mafic rocks shows that in fact, dihedral angle variation in most igneous rocks is actually created *during* their solidification, with only limited and localized sub-solidus modification.

[88] By separating syn-crystallization from sub-solidus processes we have opened the way to the use of disequilibrium dihedral angles as a speedometer for solidification as well as an indicator of the thermal history of rocks in the sub-solidus. However, there remains much work to be done. In particular we need to place constraints on the relationship between dihedral angle and the temperature-time history, both during and after solidification. We also need to quantify how the balance of crystal growth and mass transport acts to control the geometry of triple junctions during solidification, and how grain boundaries and interfaces migrate during dihedral angle modification.

Appendix A: Operating Conditions for Ti Analyses of Quartz

[89] We used a Cameca SX100 electron probe micro-analyser. The analyses used an accelerating voltage of 25 keV, with a nominal beam current of 300 nA and a beam diameter of 1 micron. The detection limit was 7 ppm Ti. The PAP corrections procedure was used for data processing and was run using Cameca Peak Sight software. The exact position of each analysis was recorded on a backscatter electron image.

References

Adamson, A. W. (1990), *Physical Chemistry of Surfaces*, 5th ed., Wiley, New York.

Almond, D. C. (1964), Metamorphism of Tertiary lavas in Strathaird, Skye, *Trans. R. Soc. Edinburgh*, *45*, 413–435.

Barth, G. A., M. C. Kleinrock, and R. T. Helz (1994), The magma body at Kilauea Iki lava lake: Potential insights into mid-ocean ridge magma chambers, *J. Geophys. Res.*, *99*, 7199–7217, doi:10.1029/93JB02804.

Bédard, J. H., R. S. J. Sparks, R. Renner, M. J. Cheadle, and M. A. Hallworth (1988), Peridotite sills and metasomatic gabbros in the eastern layered series of the Rhum complex, *J. Geol. Soc.*, *145*, 207–224, doi:10.1144/gsjgs.145.2.0207.

Bernstein, S., M. T. Rosing, C. K. Brooks, and D. K. Bird (1992), An ocean-ridge magma chamber at a passive volcanic, continental margin: The Kap Edvard Holm layered gabbro complex, East Greenland, *Geol. Mag.*, *129*, 437–456, doi:10.1017/S001675680001952X.

Bigg, E. K. (1953), The supercooling of water, *Proc. Phys. Soc. B*, *66*, 688–694.

Brown, G. M. (1956), The layered ultrabasic rocks of Rhum, Inner Hebrides, *Philos. Trans. R. Soc. B*, *240*, 1–54, doi:10.1098/rstb.1956.0011.

Butcher, A. R., I. M. Young, and J. W. Faithfull (1985), Finger structures in the Rhum complex, *Geol. Mag.*, *122*, 491–502, doi:10.1017/S001675680003541X.

Cabane, H., D. Laporte, and A. Provost (2005), An experimental study of Ostwald ripening of olivine and plagioclase in silicate melts: Implications for the growth and size of crystals in magmas, *Contrib. Mineral. Petrol.*, *150*, 37–53, doi:10.1007/s00410-005-0002-2.

Cahn, J. W. (1980), Surface stress and the chemical equilibrium of small crystals: I. The case of the isotropic surface, *Acta Metall.*, *28*, 1333–1338, doi:10.1016/0001-6160(80)90002-4.

Cesare, B., S. Ferrero, E. Salvioli-Mariani, D. Pedron, and A. Cavallo (2009), "Nanogranite" and glassy inclusions: The anatectic melt in migmatites and granulites, *Geology*, *37*, 627–630, doi:10.1130/G25759A.1.

Clemens, J. D., and M. B. Holness (2000), Textural evolution and partial melting of arkose in a contact aureole: A case study and implications, *Electron. Geosci.*, *5*, 1–14.

Deer, W. A., and D. Abbott (1965), Clinopyroxenes of the gabbro cumulates of the Kap Edvard Holm complex, East Greenland, *Min. Mag.*, *34*, 177–193.

Echebarria, B., R. Folch, A. Karma, and M. Plapp (2004), Quantitative phase-field model of alloy solidification, *Phys. Rev. E*, *70*, 061604, doi:10.1103/PhysRevE.70.061604.

Elliott, M. T., M. J. Cheadle, and D. A. Jerram (1997), On the identification of textural disequilibrium in rocks using dihedral angle measurements, *Geology*, *25*, 355–358, doi:10.1130/0091-7613(1997)025<0355:OTIOTE>2.3.CO;2.

Emeleus, C. H. (1994), *1:20 000 Solid Geology Map of Rum*, 2nd ed., Scot. Nat. Heritage, Edinburgh.

Emeleus, C. H., M. J. Cheadle, R. H. Hunter, B. G. J. Upton, and W. J. Wadsworth (1996), The Rum layered suite, in *Layered Intrusions*, edited by R. G. Cawthorn, pp. 403–439, Elsevier, Amsterdam, doi:10.1016/S0167-2894(96)80014-5.

Faure, G., and T. Mensing (2010), *The Transantarctic Mountains: Rocks, Ice, Meteorites and Water*, 830 pp., Springer, New York.

Ferry, J. M., L. J. Mutti, and G. J. Zuccala (1987), Contact metamorphism/hydrothermal alteration of Tertiary basalts from the Isle of Skye, northwest Scotland, *Contrib. Mineral. Petrol.*, *95*, 166–181, doi:10.1007/BF00381266.

Gilmer, G. H. (1976), Growth on imperfect crystal faces: I. Monte-Carlo growth rates, *J. Cryst. Growth*, *36*, 15–28, doi:10.1016/0022-0248(76)90209-8.

Gleason, G. C., V. Bruce, and H. W. Green (1999), Experimental investigation of melt topology in partially molten quartz-feldspathic aggregates under hydrostatic and non-hydrostatic stress, *J. Metamorph. Geol.*, *17*, 705–722, doi:10.1046/j.1525-1314.1999.00228.x.

Grove, T. L., M. B. Baker, and R. J. Kinzler (1984), Coupled CaAl-NaSi diffusion in plagioclase feldspar: Experiments and applications to cooling rate speedometry, *Geochim. Cosmochim. Acta*, *48*, 2113–2121, doi:10.1016/0016-7037(84)90391-0.

Hammouda, T., and D. Laporte (2000), Ultrafast mantle impregnation by carbonatite melts, *Geology*, *28*, 283–285, doi:10.1130/0091-7613(2000)28<283: UMIBCM>2.0.CO;2.

Harker, D., and E. R. Parker (1945), Grain shape and grain growth, *Trans. ASME*, *34*, 159–195.

Harte, B., R. H. Hunter, and P. D. Kinny (1993), Melt geometry, movement and crystallization, in relation to mantle dykes, veins and metasomatism, *Philos. Trans. R. Soc. A*, *342*, 1–21, doi:10.1098/rsta.1993.0001.

Helz, R. T. (1987), Differentiation behavior of Kilauea Iki lava lake, Kilauea volcano, Hawaii: An overview of past and current work, in *Magmatic Processes: Physicochemical Principles*, edited by B. O. Mysen, *Spec. Publ. Geochem. Soc.*, *1*, 241–258.

Helz, R. T. (2009), Processes active in mafic magma chambers: The example of Kilauea Iki lava lake, Hawaii, *Lithos*, *111*, 37–46, doi:10.1016/j. lithos.2008.11.007.

Helz, R. T., and C. R. Thornber (1987), Geothermometry of Kilauea Iki lava lake, Hawaii, *Bull. Volcanol.*, *49*, 651–668, doi:10.1007/BF01080357.

Helz, R. T., N. G. Banks, T. J. Casadevall, R. S. Fiske, and R. B. Moore (1984), A catalogue of drill core recovered from Kilauea Iki lava lake from 1967 to 1979, *U.S. Geol. Surv. Open File Rep.*, *84–484*, 72 pp.

Higgins, M. D. (2011), Textural coarsening in igneous rocks, *Int. Geol. Rev.*, *53*, 354–376, doi:10.1080/00206814.2010.496177.

Holness, M. B. (2005), Spatial constraints on magma chamber replenishment events from textural observations of cumulates: The Rum layered intrusion, Scotland, *J. Petrol.*, *46*, 1585–1601, doi:10.1093/petrology/egi027.

Holness, M. B. (2006), Melt-solid dihedral angles of common minerals in natural rocks, *J. Petrol.*, *47*, 791–800, doi:10.1093/petrology/egi094.

Holness, M. B. (2007), Textural immaturity of cumulates as an indicator of magma chamber processes: Infiltration and crystal accumulation in the Rum eastern layered intrusion, *J. Geol. Soc.*, *164*, 529–539, doi:10.1144/0016-76492006-021.

Holness, M. B. (2010), Decoding dihedral angles in melt-bearing and solidified rocks, *J. Virtual Explor.*, *35*, 3, doi:10.3809/jvirtex.2010.00265.

Holness, M. B., and M. C. S. Humphreys (2003), The Traigh Bhàn na Sgùrra sill, Isle of Mull: Flow localization in a major magma conduit, *J. Petrol.*, *44*, 1961–1976, doi:10.1093/petrology/egg060.

Holness, M. B., and E. W. Sawyer (2008), On the pseudomorphing of melt-filled pores during the crystallization of migmatites, *J. Petrol.*, *49*, 1343–1363, doi:10.1093/petrology/egn028.

Holness, M. B., and S. T. C. Siklos (2000), The rates and extent of textural equilibration in high-temperature fluid-bearing systems, *Chem. Geol.*, *162*, 137–153, doi:10.1016/S0009-2541(99)00124-2.

Holness, M. B., and B. Winpenny (2009), The unit 12 allivalite, eastern layered intrusion, Isle of Rum: A textural and geochemical study of an open-system magma chamber, *Geol. Mag.*, *146*, 437–450, doi:10.1017/S0016756808005797.

Holness, M. B., M. J. Bickle, and B. Harte (1989), Textures of forsterite-calcite marbles from the Beinn an Dubhaich aureole, Skye, and implications for the structure of metamorphic porosity, *J. Geol. Soc.*, *146*, 917–920, doi:10.1144/gsjgs.146.6.0917.

Holness, M. B., M. J. Bickle, and C. M. Graham (1991), On the kinetics of textural equilibration in forsterite marbles, *Contrib. Mineral. Petrol.*, *108*, 356–367, doi:10.1007/BF00285943.

Holness, M. B., M. J. Cheadle, and D. McKenzie (2005a), On the use of changes in dihedral angle to decode late-stage textural evolution in cumulates, *J. Petrol.*, *46*, 1565–1583, doi:10.1093/petrology/egi026.

Holness, M. B., V. M. Martin, and D. M. Pyle (2005b), Information about open-system magma chambers derived from textures in magmatic enclaves: The Kameni Islands, Santorini, Greece, *Geol. Mag.*, *142*, 637–649, doi:10.1017/S0016756805001172.

Holness, M. B., T. F. D. Nielsen, and C. Tegner (2007a), Textural maturity of cumulates: A record of chamber filling, liquidus assemblage, cooling rate and large-scale convection of mafic layered intrusions, *J. Petrol.*, *48*, 141–157, doi:10.1093/petrology/egl057.

Holness, M. B., C. Tegner, T. F. D. Nielsen, G. Stripp, and S. A. Morse (2007b), A textural record of solidification and cooling in the Skaergaard intrusion, East Greenland, *J. Petrol.*, *48*, 2359–2377, doi:10.1093/petrology/egm064.

Holness, M. B., A. T. Anderson, V. M. Martin, J. Maclennan, E. Passmore, and K. Schwindinger (2007c), Textures in partially solidified crystalline nodules: A window into the pore structure of slowly cooled mafic intrusions, *J. Petrol.*, *48*, 1243–1264, doi:10.1093/petrology/egm016.

Holness, M. B., M. A. Hallworth, A. Woods, and R. E. Sides (2007d), Infiltration metasomatism of cumulates by intrusive magma replenishment: The wavy horizon, Isle of Rum, Scotland, *J. Petrol.*, *48*, 563–587, doi:10.1093/petrology/egl072.

Holness, M. B., G. Stripp, M. C. S. Humphreys, I. V. Veksler, T. F. D. Nielsen, and C. Tegner (2011), Silicate liquid immiscibility within the

crystal mush: Late-stage magmatic microstructures in the Skaergaard Intrusion, East Greenland, *J. Petrol.*, *52*, 175–222, doi:10.1093/petrology/egq077.

Humphreys, M. C. S. (2009), Chemical evolution of intercumulus liquid, as recorded in plagioclase overgrowth rims from the Skaergaard intrusion, *J. Petrol.*, *50*, 127–145, doi:10.1093/petrology/egn076.

Humphreys, M. C. S. (2011), Silica liquid immiscibility within the crysta mush: Evidence from Ti in plagioclase from the Skaergaard intrusion, *J. Petrol.*, *52*, 147–174, doi:10.1093/petrology/egq076.

Huppert, H. E., and R. S. Sparks (1981), The fluid dynamics of a basaltic magma chamber, replenished by hot, dense, ultrabasic magma, *Contrib. Mineral. Petrol.*, *75*, 279–289, doi:10.1007/BF01166768.

Kays, M. A., G. G. Goles, and T. W. Grover (1989), Precambrian sequence bordering the Skaergaard Intrusion, *J. Petrol.*, *30*, 321–361.

Kirkpatrick, R. J. (1975), Crystal growth from the melt: A review, *Am. Mineral.*, *60*, 798–814.

Kirkpatrick, R. J. (1976), Towards a kinetic model for the crystallization of magma bodies, *J. Geophys. Res.*, *81*, 2565–2571, doi:10.1029/JB081i014p02565.

Kirkpatrick, R. J. (1981), Kinetics of crystallization of igneous rocks, *Rev. Mineral. Geochem.*, *8*, 321–398.

Kirkpatrick, R. J., G. R. Robinson, and J. F. Hayes (1976), Kinetics of crystal growth from silicate melts: Anorthite and diopside, *J. Geophys. Res.*, *81*, 5715–5720, doi:10.1029/JB081i032p05715.

Kruhl, J. H. (2001), Crystallographic control on the development of foam textures in quartz, plagioclase and analogue material, *Int. J. Earth Sci.*, *90*, 104–117, doi:10.1007/s005310000170.

Kruhl, J. H., and M. Peternell (2002), The equilibration of high-angle grain boundaries in dynamically recrystallised quartz: The effect of crystallography and temperature, *J. Struct. Geol.*, *24*, 1125–1137, doi:10.1016/S0191-8141(01)00096-7.

Larsen, R. B., and C. Tegner (2006), Pressure conditions for the solidification of the Skaergaard intrusion: Eruption of East Greenland flood basalts in less than 300,000 years, *Lithos*, *92*, 181–197, doi:10.1016/j.lithos.2006.03.032.

Liebl, C., B. Kuntcheva, J. R. Kruhl, and K. Kunze (2007), Crystallographic orientations of quartz grain-boundary segments formed during dynamic recrystallisation and subsequent annealing, *Eur. J. Mineral.*, *19*, 735–744, doi:10.1127/0935-1221/2007/0019-1759.

Maclennan, J., D. McKenzie, K. Gronvold, N. Shimizu, J. M. Eiler, and N. Kitchen (2003), Melt mixing and crystallisation under Theistareykir, northeast Iceland, *Geochem. Geophys. Geosyst.*, *4*(11), 8624, doi:10.1029/2003GC000558.

Marchildon, N., and M. Brown (2002), Grain-scale melt distribution in two contact aureole rocks: Implications for controls on melt localization and deformation, *J. Metamorph. Geol.*, *20*, 381–396, doi:10.1046/j.1525-1314.2002.00376.x.

Martin, V. M., M. B. Holness, and D. M. Pyle (2006), Textural analysis of magmatic enclaves from the Kameni Islands, Santorini, Greece, *J. Volcanol. Geotherm. Res.*, *154*, 89–102, doi:10.1016/j.jvolgeores.2005.09.021.

Means, W. D., and Y. Park (1994), New experimental approach to understanding igneous texture, *Geology*, *22*, 323–326, doi:10.1130/0091-7613(1994)022<0323:NEATUI>2.3.CO;2.

Melia, T. P., and W. P. Moffitt (1964), Crystallisation from aqueous solution, *J. Colloid Sci.*, *19*, 433–447, doi:10.1016/0095-8522(64)90043-1.

Morse, S. A., and K. M. Nolan (1984), Origin of strongly reversed rims on plagioclase in cumulates, *Earth Planet. Sci. Lett.*, *68*, 485–498, doi:10.1016/0012-821X(84)90132-8.

Morse, S. A., B. E. Owens, and A. R. Butcher (1987), Origin of finger structures in the Rhum complex–Phase equilibrium and heat effects, *Geol. Mag.*, *124*, 205–210, doi:10.1017/S0016756800016241.

Ostwald, W. (1901), *Analytisch Chemie*, 3rd ed., Engelman, Leipzig, Germany.

Philpotts, A. R. (1963), Petrology of the Morin Series in southern Quebec, PhD thesis, Univ. of Cambridge, Cambridge, U. K.

Philpotts, A. R., J. Shi, and C. Brustman (1998), Role of plagioclase crystal chains in the differentiation of partly crystallized basaltic magma, *Nature*, *395*, 343–346, doi:10.1038/26404.

Platten, I. M. (1982), Partial melting of feldspathic quartzite around late Caledonian minor intrusions in Appin, Scotland, *Geol. Mag.*, *119*, 413–419, doi:10.1017/S0016756800026327.

Putnis, A., and G. Mauthe (2001), The effect of pore size on cementation in porous rocks, *Geofluids*, *1*, 37–41, doi:10.1046/j.1468-8123.2001.11001.x.

Rappaz, M., A. Jacot, and W. J. Boettinger (2003), Late-stage solidification of alloys: Theoretical model of dendrite-arm and grain coalescence, *Metall. Mater. Trans. A*, *34*, 467–479.

Richter, D. H., J. P. Eaton, K. J. Murata, W. U. Ault, and H. L. Krivoy (1970), Chronological narrative of the 1959–1960 eruption of Kilauea Volcano, Hawaii, *U.S. Geol. Surv. Prof. Pap.*, *537-E*, 70 pp.

Riegger, O. K., and L. H. van Vlack (1960), Dihedral angle measurements, *Metall. Trans.*, *21*, 933–935.

Roselle, G. T., L. P. Baumgartner, and J. A. Chapman (1997), Nucleation-dominated crystallization of forsterite in the Ubehebe Peak contact aureole, *Calif. Geol.*, *25*, 823–826.

Sawyer, E. W. (1999), Criteria for the recognition of partial melting, *Phys. Chem. Earth, Part A*, *24*, 269–279.

Scherer, G. W. (1999), Crystallisation in pores, *Cement Concr. Res.*, *29*, 1347–1358, doi:10.1016/S0008-8846(99)00002-2.

Sides, R. (2008), Crystal mushes in mafic magma chambers, PhD thesis, Univ. of Cambridge, Cambridge, U. K.

Stanton, R. L., and H. Gorman (1968), Annealing of single phase poly crystalline sulphide ores, *Nature*, *217*, 160–162, doi:10.1038/217160a0.

Stevenson, D. J. (1986), On the role of surface tension in the migration of melts and fluids, *Geophys. Res. Lett.*, *13*, 1149–1152, doi:10.1029/GL013i011p01149.

Stickels, C. A., and E. E. Hücke (1964), Measurement of dihedral angles, *Metall. Trans.*, *230*, 795–801.

Tait, S. R. (1984), Fluid dynamical processes in the formation of layered igneous rocks, PhD thesis, Univ. of Cambridge, Cambridge, U. K.

Tait, S. R. (1985), Fluid dynamic and geochemical evolution of cyclic unit 10, Rhum, eastern layered series, *Geol. Mag.*, *122*, 469–484, doi:10.1017/S0016756800035391.

Tegner, C., and J. R. Wilson (1995), Textures in a poikilitic olivine gabbro cumulate: Evidence for supercooling, *Mineral. Petrol.*, *54*, 161–173, doi:10.1007/BF01162859.

Tegner, C., J. R. Wilson, and C. K. Brooks (1993), Intraplutonic quench zones in the Kap Edvard Holm Layered Gabbro Complex, East Greenland, *J. Petrol.*, *34*, 681–710.

Tegner, C., P. Thy, M. B. Holness, J. K. Jakobsen, and C. E. Lesher (2009), Differentiation and compaction in the Skaergaard Intrusion, *J. Petrol.*, *50*, 813–840, doi:10.1093/petrology/egp020.

Toplis, M. J., W. L. Brown, and E. Pupier (2008), Plagioclase in the Skaergaard intrusion. Part 1: Core and rim compositions in the layered series, *Contrib. Mineral. Petrol.*, *155*, 329–340, doi:10.1007/s00410-007-0245-1.

Tracy, R. J., and B. R. Frost (1991), Phase equilibria and thermobarometry of calcareous, ultramafic and mafic rocks, and iron formations, *Rev. Mineral.*, *26*, 207–290.

Vernede, S., and M. Rappaz (2007), A simple and efficient model for meso-scale solidification simulation of globular grain structures, *Acta Mater.*, *55*, 1703–1710, doi:10.1016/j.actamat.2006.10.031.

Vernon, R. H. (1968), Microstructures of high-grade metamorphic rocks at Broken Hill, Australia, *J. Petrol.*, *9*, 1–22.

Vernon, R. H. (1970), Comparative grain-boundary studies of some basic and ultrabasic granulites, nodules and cumulates, *Scott. J. Geol.*, *6*, 337–351, doi:10.1144/sjg06040337.

Vernon, R. H. (2004), *A Practical Guide to Rock Microstructure*, 594 pp., Cambridge Univ. Press, Cambridge, U. K.

Voll, G. (1960), New work on petrofabrics, *Liverpool Manchester Geol. J.*, *2*, 503–567.

Voll, G. (1969), Klastische Mineralien aus den Sedimentserien der Schottischen Highlands und ihr Schicksal bei aufsteigender Regional-und Kontaktmetamorphose. Habilitationsschrift, Fakultät für Bergbau und Huttenwesen, diploma thesis, Tech. Univ. of Berlin, Berlin.

Wark, D. A., and E. B. Watson (2006), The TitaniQ: A titanium-in-quartz geothermometer, *Contrib. Mineral. Petrol.*, *152*, 743–754, doi:10.1007/s00410-006-0132-1.

Wartho, J.-A., S. P. Kelley, and S. Blake (2001), Magma flow regimes in sills deduced from Ar-isotope systematics of host rocks, *J. Geophys. Res.*, *106*, 4017–4035, doi:10.1029/2000JB900327.

Watson, E. B. (1982), Melt infiltration and magma evolution, *Geology*, *10*, 236–240, doi:10.1130/0091-7613(1982)10<236:MIAME>2.0.CO;2.